

# **Precise Somatotopic Thalamocortical Axon Guidance Depends on LPA-Mediated PRG-2/Radixin Signaling**

A dissertation submitted to attain the academic degree of

**Doctor of Philosophy (Ph.D.)**

from the Faculties  
University Medical Center,  
Social Sciences, Media, and Sports,  
Chemistry, Pharmaceutical Sciences, and Geosciences,  
and  
Biology  
of the Johannes Gutenberg University Mainz

Jin Cheng  
Born 01.10.1984 in Hubei, PR China

The present work was performed from March 2013 to October 2016 in the Institute of Microanatomy and Neurobiology.

**Date of Examination:** 20.01.2017

## Zusammenfassung auf Deutsch

Eine präzise Verknüpfung von Axonen ist für die Funktion des Nervensystems unabdingbar. Während der embryonalen Gehirnentwicklung wandern thalamokortikale Axone (TCA) durch das ventrale Telencephalon und gelangen durch die Intermediärzone (IZ) zu ihrem Zielgebiet im telencephalen Kortex. Die TCA warten in der IZ bis zum letzten Stadium der embryonalen Entwicklung, bevor sie beginnen die kortikale Platte (CP) zu innervieren und Verknüpfungen mit den Neuronen der Schicht IV zu bilden.

In dieser Studie wurde gezeigt, dass das PRG-2 Protein (PRG-2, plasticity related gene 2), welches in den TCAs exprimiert wird, von großer Bedeutung für das Verbleiben der TCAs in der IZ ist und ein vorzeitiges und aberrantes Einwandern der TCA in die CP bereits im frühen embryonalen Stadium (E16) verhindert.

Die zugrunde liegenden molekularen Mechanismen, welche in dieser Doktorarbeit untersucht wurden zeigen, dass das Molekül PRG-2 welches in den Wachstumskegeln (GCs, growth cones) exprimiert wird, eine Abstoßungsreaktion auf Lysophosphatidsäure (LPA) vermittelt.

PRG-2 knock-out Axone sind dagegen gegenüber LPA, welches von der Subplatte produziert wird, nicht empfindlich. Die Subplatte liegt unterhalb der CP.

Die vorliegenden Ergebnisse zeigen, dass die Neurone der Subplatte eine wichtige Rolle bei der korrekten somatotopischen Termination der TCA spielen.

Die weitere Erforschung der Signaltransduktionswege zeigte, dass PRG-2 mit Radixin (RDX) interagiert und die Phosphorylierung von RDX nach LPA-Stimulation vermittelt.

Die LPA/PRG-2/pRDX Signaltransduktionsachse führt zu Änderungen im Aktin-Zytoskelett in den GCs thalamokortikaler Axone. Zusammenfassend konnte gezeigt werden, dass die somatotopische Termination der TCA über die LPA-vermittelten PRG-2/RDX Signaltransduktion vermittelt wird.

Stichworte: PRG-2, LPA, thalamokortikale Axone, axonale Führung/Lenkung, Radixin

## Abstract

The function of the nervous system relies to the precision of axon wiring. During embryonic brain development, thalamocortical axons (TCAs) navigate through the ventral telencephalon to reach the intermediate zone (IZ) of the cerebral cortex. TCAs wait in the IZ until the late embryonic stage before they start to innervate the cortical plate (CP) and to form connections with layer IV neurons.

This study discovered that the plasticity related gene protein 2 (PRG-2), which is expressed at TCAs, is critically important to maintain TCAs in the IZ and prevents a premature and aberrant entrance of TCA into the CP at the early embryonic day 16 (E16). To explore the underlying molecular mechanism, TCAs growth behaviors are observed *in vitro* cultures. TCAs show a repulsive response to lysophosphatidic acid (LPA) via PRG-2 present in their growth cones (GCs). However, PRG-2 knock-out fibers lose sensitivity to the guidance cue LPA, which is produced by the subplate-secreted autotaxin (ATX) in developing brains. The results suggest that subplate neurons play a major role in the guidance of TCAs development.

Further signaling pathway research shows that PRG-2 interacts with Radixin (RDX) and mediates RDX phosphorylation upon LPA-stimulation. Consequently, PRG-2/pRDX axis coordinates actin cytoskeleton changes in GCs of thalamocortical axons in response to LPA. In sum, precise somatotopic termination of TCAs critically depends on LPA-mediated PRG-2/RDX signaling.

Keywords: PRG-2, LPA, thalamocortical axons, axonal guidance, Radixin

## List of abbreviations

ENPPs	ectonucleotidepyrophosphatase/ phosphodiesterases
LPR/PRGs	lipid phosphatase-related proteins/plasticity-related genes
LPPs	lipid phosphate phosphatases
POm	posterior medial
SMSs	sphingomyelin synthases
SPPs	sphingosine phosphate phosphatases
SPC	sphingosylphosphoryl choline
TG	the trigeminal ganglion
ATX	autotaxin
SpVi	brainstem trigeminal complex
CP	cortical plate
PSPB	diencephalic–telencephalic boundary
E	embryonic day
ERM	Ezrin-Radixin-Moesin
GCs	growth cones
IHC	immunohistochemistry
IP	Immunoprecipitation
IZ	intermediate zone
IC	internal capsule
LPTs	Lipid phosphatases/phosphotransferases
LPA-Rs	LPA receptors
LPA	lysophosphatidic acid
LPC	lysophosphatidylcholine
LPs	lysophospholipids
DTB	pallial–subpallial boundary
PIP2	phosphatidylinositol 4,5-bisphosphate
PLD	phospholipase D
PRG-2	plasticity related gene protein 2
P	postnatal day
S1	primary somatosensory cortex
PrV	principal sensory nucleus
RDX	radixin
RFP	red fluorescent protein
RTN	reticular thalamic nucleus
S1P	sphingosine 1-phosphate
TCAAs	thalamocortical axons
ION	The infraorbital nerve
CSS2s	type 2 candidate sphingo-myelin synthases
VPM	ventral posteromedial
VZ	ventricular zone

# Table of Contents

Zusammenfassung auf Deutsch .....	1
Abstract .....	2
List of abbreviations .....	3
Table of Contents .....	4
1 Introduction.....	6
1.1 PRG-2 and LPA signaling pathway .....	6
1.2 Early development of thalamocortical projections.....	10
1.3 Guidance cues .....	12
2 Materials and Methods .....	16
2.1 Mouse mutants and tamoxifen injection.....	16
2.2 Immunofluorescent stainings (IF).....	16
2.3 Anterograde and retrograde tracing .....	17
2.4 Cytochrome oxidase staining .....	17
2.5 Slice culture, biocytin labeling and slice electroporation.....	18
2.6 Thalamic and cortical explants .....	18
2.7 Preparation of hippocampic neuron culture.....	19
2.8 Live imaging of RDX distribution in the GC.....	20
2.9 Analysis of pERM distribution in GC.....	20
2.10 Analysis of pERM expression in dissociated neurons.....	20
2.11 Preparation thalamic neuron culture and GC collapse assay.....	21
2.12 Quantitative PCR .....	21
2.13 Statistics.....	22
3 Results .....	23
3.1 <i>PRG-2</i> is expressed in developing brains.....	23
3.2 <i>PRG-2</i> knock-out mice have a defect in thalamocortical projection.....	26
3.3 <i>PRG-2</i> is functionally required in thalamocortical afferents for correct targeting .....	33
3.4 Thalamus-specific <i>PRG-2</i> knock-out mice have a defect in the thalamocortical projection...	36

3.5 LPA signaling is critical for TCAs guidance in PRG-2 <sup>-/-</sup> mice.....	42
3.6 PRG-2 mediates axonal sensitivity to LPA .....	47
3.7 Radixin (RDX) is a downstream PRG-2 interacting molecule in the axon GC.....	53
3.8 PRG-2 mediates pERM increase at GC membranes induced by extracellular LPA.....	57
3.9 RDX-deficiency phenocopies PRG-2 thalamocortical axon defect.....	63
4 Discussion .....	66
References.....	69
Curriculum vitae .....	76
List of own publications.....	78
Acknowledgements.....	80
Declarations.....	81

# 1 Introduction

Plasticity related genes (PRGs) are a phospholipid interacting group of molecules involved in neuronal homeostasis during brain development and in neuronal adaptation to plastic changes of the nervous system (Brauer and Nitsch, 2008; Brauer et al., 2003; Trimbuch et al., 2009). The goal of this study was to investigate the role of PRG-2, a PRG-family member expressed at embryonic brains. Until now, the function of PRG-2 was unknown yet. This study started with the characteristic of PRG-2 protein expression and the known hints from its homology protein and adopted thalamocortical pathfinding as the model to uncover the role of PRG-2 in the developmental brains.

## 1.1 PRG-2 and LPA signaling pathway

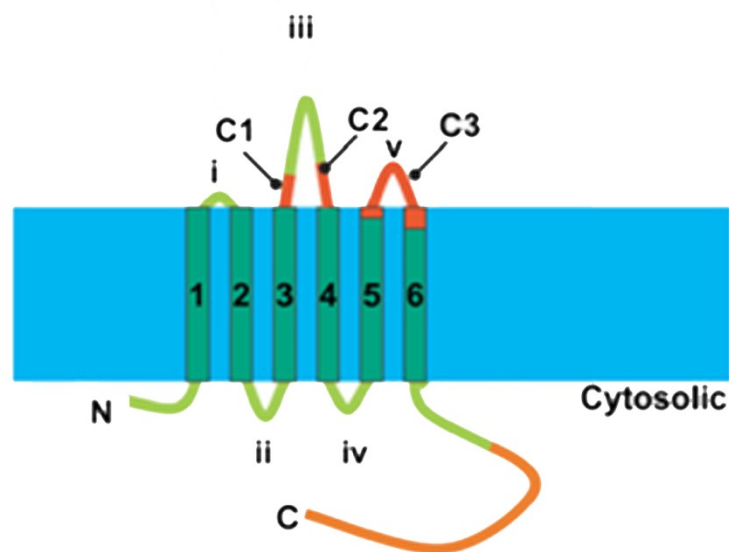
The lipids in human can be utilized into two parts, structure and signaling. The most abundant membrane lipids are the phospholipids, containing hydrophilic head group and hydrophobic tails. The majority of phospholipids in most cell membranes are phosphoglycerides and sphingolipids. They are metabolized into polar metabolites such as eicosanoids and lysophospholipids (LPs). These LPs include lysophosphatidic acid (LPA), lysophosphatidylcholine (LPC), sphingosylphosphoryl choline (SPC), and sphingosine 1-phosphate (S1P), which play critical roles in signal transduction, intracellular membrane trafficking, and control of cell growth and survival (Hla et al., 2001).

Lipid phosphatases/phosphotransferases (LPTs) are a family of integral membrane proteins which modulate bioactive lipid metabolism and signaling. LPTs consist of five groups of homologous protein which are LPPs (lipid phosphate phosphatases), SPPs (sphingosine phosphate phosphatases), SMSs (sphingomyelin synthases), CSS2s (type 2 candidate sphingo-myelin synthases) and LPR/PRGs (lipid phosphatase-related proteins/plasticity-related genes) (Sigal et al., 2005; Stuke and Carman, 1997).

It has been discovered that three conserved active site domains of LPP play a critical role in lipid phosphates hydrolyzation. Hence, LPPs can dephosphorylate intracellularly generated substrates to control intracellular lipid metabolism and signaling. Meanwhile, they regulate cell surface receptor-mediated signaling by LPA and S1P by inactivating these lipids near the



plasma membrane and extracellular matrix (Sigal et al., 2005; Stukey and Carman, 1997). When [<sup>32</sup>P]LPA was injected into the bloodstream of mice, the half-life of LPA in the blood was about 12 mins in LPP1-deficient mice compared with 3 mins in WT (Tomsig et al., 2009). In comparison with other members of the LPT family, PRGs is far less studied. Although PRGs and LPPs both possess six transmembrane domains, PRGs lack conserved critical amino acids within the catalytic site (Sigal et al., 2005; Stukey and Carman, 1997) (Figure 1.1). Hence, there is a reason to believe that PRGs have evolved to a protein family bearing additional functions when compared to LPPs.



Phosphatase	C1	C2	C3
Consensus:	KXXXXXXXXRP	SGH	SRXXXXXXXXHXXD
LPP1	(125) KYSIGRLRP	(174) SGH	(221) SRVSDYKHHWSD
LPP2	(117) KYMIGRLRP	(166) SGH	(213) TRVSDYKHHWSD
LPP3	(148) KVSIGRLRP	(197) SGH	(244) SRVSDHKHHPSD
LPR1/PRG3	(146) PYFLTVC <u>K</u> P	(198) S <u>K</u> H	(245) NRVSEYRN <u>H</u> CSD
LPR2/PRG4	(148) PHFLSV <u>C</u> RP	(207) C <u>K</u> D	(154) VRVAEYRN <u>H</u> WSD
LPR3/PRG1	(197) Q <u>L</u> STGYQ <u>A</u> P	(250) S <u>Q</u> H	(296) TRITQYKN <u>H</u> PVD
LPR4/PRG2	(152) Q <u>L</u> ATGYHT <u>P</u>	(205) S <u>Q</u> H	(279) TQITQYR <u>S</u> HPVD

Figure 1.1 PRGs lack conserved amino acids within the catalytic site as LPPs (Sigal et al., 2005)

PRGs have increasingly attracted interest after Brauer *et al.* (2003) firstly identified PRG-1 by differential screening of a cDNA library from lesioned hippocampus (Brauer et al., 2003). Five

members of PRGs family (PRG1-5) have highly conserved transmembrane domains. Within the family, PRG1 was widely studied. It has been published that PRG1 attenuates phospholipid-induced axon collapse in neurons and facilitates outgrowth in the hippocampus (Brauer et al., 2003). In adult mice, PRG1 locates at the postsynaptic density and is responsible for the transduction and modulation of glutamatergic signaling (Trimbuch et al., 2009). Meanwhile, PRG1- deficiency reduces spine numbers, alters long-term potentiation, and impairs spatial memory (Liu et al., 2016).

According to the homology of PRG2, the studies of PRG-1 help to understand the function of the PRG-2. However, there are significant differences in their spatiotemporal expression. PRG-2 protein can be detected at embryonic day 12 (E12), which mainly locates in the ventricular zone (VZ) of the neocortex. Subsequently, the expression is decreased in VZ, and thalamocortical fibers from dorsal diencephalon strongly express at E14. Those evidences provide a hint that PRG-2 might play a role in the developmental brain. PRG-1 transcripts are detected in the brain until E19 in the subventricular zone and specifically in the hippocampal anlage, whereas other cortical regions did not show *PRG-1* expression. From postnatal stages on, PRG-1 mRNA was present in the hippocampus and the entorhinal cortex. This expression pattern remains unchanged during maturation; however, a reduced expression is apparent in the adult brain (Brauer et al., 2003).

In summary, PRG-2 lacks critical amino acids with the function to dephosphorylate lysophospholipids like LPP and has different expression pattern to its family member, PRG-1. Nevertheless, the discoveries at least express a hint that PRG-2 is a LPA-interacting protein.

It is well studied that LPA signals mediate neuron processes such as survival, proliferation, differentiation and migration, which is mainly mediated by LPA receptors (LPA-Rs) in the developing brain (Contos et al., 2000; Estivill-Torrus et al., 2008; Kingsbury et al., 2003). LPA-Rs are seven-transmembrane GPCRs binding different LPA subspecies with varying affinities and activate specific heterotrimeric G protein pathways via  $G\alpha_{12/13}$ ,  $G\alpha_{q/11}$ ,  $G\alpha_{i/o}$  and  $G\alpha_s$ . The downstream signaling cascades involve in Ras, Rho, Rac, Akt, MAPK, PKC and adenylate cyclase (reviewed by (Sheng et al., 2015; Yung et al., 2015)).

One of the most important actions of LPA is its function as a repellent factor for axons, eventually leading to GC collapse (Campbell and Holt, 2001). Compared to another repulsive

guidance cue Semaphorin 3A, translation machinery is not involved in the process of LPA-induced collapse. Yuan *et al.* showed that the repulsive action of LPA depended on the activity of RhoA but not Cdc42 (Yuan et al., 2003). However, the point of view that LPA-Rs mediate LPA-induced collapse is rather controversial, and there is no general agreement that LPA-induced GC repulsion clearly depends on the downstream LPA-Rs signaling. On the one hand, LPA-Rs mediate embryonic chick retinal GC collapse induced by LPA (Fincher et al., 2014). On the other hand, some authors from the same lab reported deletion LPA<sub>1-3</sub>-Rs were not required for the inhibitory effects of LPA on mouse retinal GC (Birgbauer and Chun, 2010). Together, this suggests the additional LPA-dependent signaling pathways independent of LPA receptors. Given these data, PRG-2 can be regarded as a possible interacting protein of extracellular LPA.

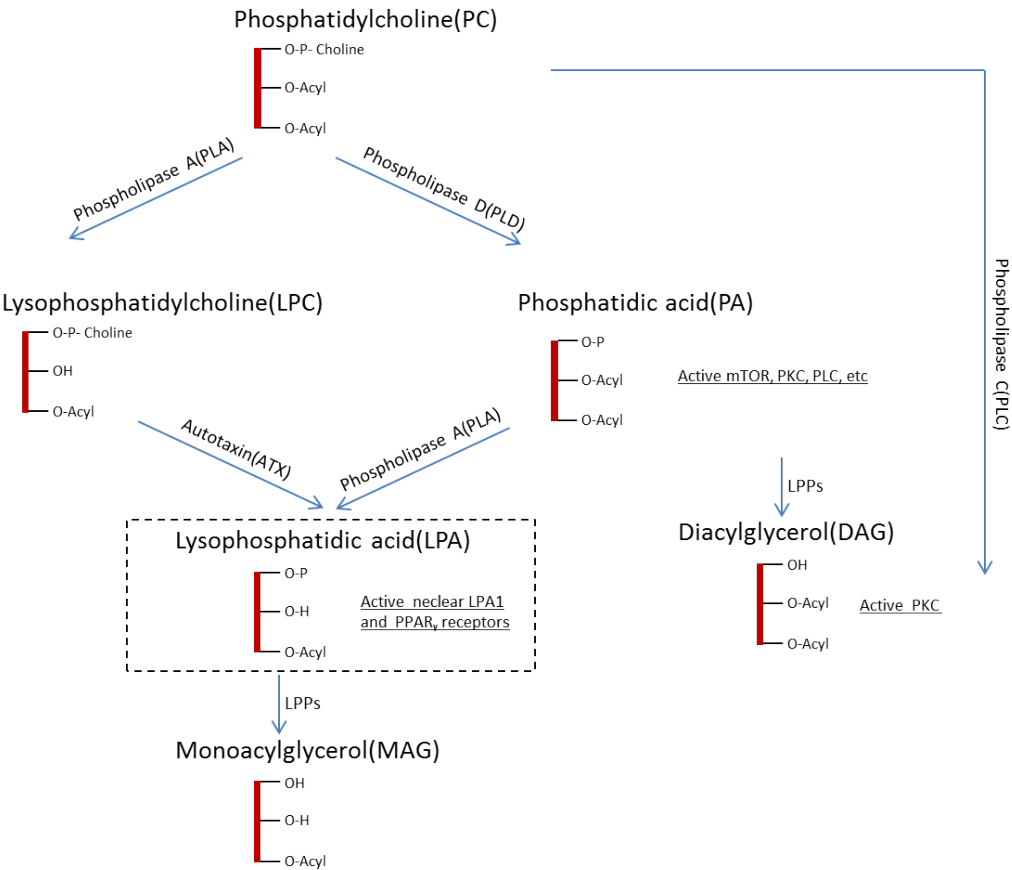


Figure 1.2 Metabolism of extracellular and intracellular bioactive lipids

To study the function of PRG-2 in the developing brain, LPA metabolism has to be mentioned. LPA can be produced in two different ways. In the first pathway, the precursor phospholipids (phosphatidylcholine, phosphatidylserine, or phosphatidylethanolamine) can be converted to their corresponding lysophospholipids such as LPC, LPS, or LPE. Lysophospholipids can then be transformed to LPA via ATX (Figure 1.2). In the second major pathway, phosphatidic acid (PA) is first produced from phospholipids through phospholipase D (PLD). Then, PA is converted directly to LPA by the actions of either PLA1 or PLA2 (Brindley and Pilquill, 2009; Mills and Moolenaar, 2003; Morris and Smyth, 2014; Yung et al., 2014; Yung et al., 2015).

ATX is a secreted enzyme as a member of the ENPPs (ectonucleotidopyrophosphatase/phosphodiesterases) family. ATX is considered as the major synthesizing enzyme for extracellular LPA. It was reported that mice deficient in ATX had an early embryonic lethality resulting from vascular defects in yolk sac. In addition, other defects including malformations in the allantois and neural tube also were reported (Tanaka et al., 2006). Greenman *et al.* revealed that ATX had a strong expression in the VZ and CP of cortex at mouse E14 brain, and was expressed throughout cortical development by Western blot analysis (Greenman et al., 2015). ATX is also expressed in the subplate neurons as shown by both in situ hybridization and a GFP reporter mouse line (Hoerder-Suabedissen et al., 2013).

## **1.2 Early development of thalamocortical projections**

Each of the sensory systems appears to begin functioning at a different stage of development, with somatosensory sensitivity emerging first and visual last. According to the PRG-2 expression pattern that presents strongly in thalamocortical fibers, the embryonic development of somatosensory circuit was selected to study PRG-2 function. The tactile somatosensory pathway from whisker to cortex in rodents provides a well-defined system for exploring the link between molecular mechanisms, synaptic circuits, and behavior.

Around E13, the neocortex and dorsal thalamus starts to innervate each other through reciprocal connections. ‘Handshake hypothesis’ postulates that projections from the early-born cortical neurons have a waiting period at this time point. Until thalamocortical fibers project through diencephalic–telencephalic boundary (PSPB) and into striatum later on, they meet corticothalamic projections at the pallial–subpallial boundary (DTB) (Deck et al., 2013).

Lopez-Bendito *et al.* reported that early interneurons tangentially migrating from the ventral telencephalon form a corridor to navigate the thalamocortical fibers through the striatum without innervation into the globus pallidus (Lopez-Bendito *et al.*, 2006).

When a major part of thalamocortical projections arrive at E16 neocortex, they accumulate in the upper layer of IZ and start to innervate the CP at P0. Subplate neurons have been long described to be involved in guiding the thalamocortical to the cortex. The *fezl*-deficient mice display a reduced number of subplate neurons, which lead to aberrant TCA (Hirata *et al.*, 2004). During the first two days after birth in mice, thalamic axons grow through the lower layers of the primary somatosensory cortex to form arbors in a periphery-related pattern. Subsequently, TCA terminals from the ventral posteromedial (VPM) nucleus are clustered to form the barrel center in cortical layer 4 (Yamasaki *et al.*, 2014). It has been reported that only 20% of the mouse pups had an established thalamocortical afferent pattern in the barrel cortex at P4, while the majority of the pups showed a well-established pattern at P5-7 (Erzurumlu and Gaspar, 2012; Hoerder-Suabedissen *et al.*, 2008). Meanwhile, L4 spiny stellate neurons (barrel cells) locate on the barrel edge, and dendrites of barrel cells are asymmetrically oriented toward the barrel center (Mizuno *et al.*, 2014). Neighboring barrels are separated from each other by narrower zones called “septa”. The polarized dendritic orientation of barrel cells becomes apparent at P6 (Erzurumlu and Gaspar, 2012).

Barrel cells receive synaptic contacts from segregated groups of thalamic axon terminals. The understanding the formation of the barrels can lead to a considerable insight into the interactions between thalamocortical projections and the cortex. Firstly, barrels formation is influenced by the inputs from the whiskers during the neonatal stage. Many studies have shown that glutamate release and serotonergic regulation are critical to barrel formation (Xu *et al.*, 2004; Yamasaki *et al.*, 2014). Organ maturation also affects the whiskers input (Hoerder-Suabedissen *et al.*, 2008). Secondly, aspects of cortical development, e.g. the layer-dependent pattern of cortical cytoarchitecture, gene expression, and neuronal differentiation depend on thalamocortical neurotransmission and other activity-dependent factors (Li *et al.*, 2013).

The primary somatosensory cortex (S1) contains a complete body map that mirrors the subcortical maps developed by peripheral sensory input (Petersen, 2014). The infraorbital

nerve (ION) of the trigeminal ganglion (TG) relays the whisker-related information from the peripheral nervous system of the whisker pad to the principal sensory nucleus (PrV) in the brain stem. Among them, the PrV-based lemniscal pathway and the interpolarissub nucleus of the brainstem trigeminal complex (SpVi)-based paralemniscal pathway as two parallel pathways respectively deliver whisker-related information to VPM and posterior medial (POm) thalamic nucleus, which then are relayed into S1 and S2 by thalamocortical axons. (Erzurumlu et al., 2006; Pouchelon et al., 2012; Yamakado, 1995).

### **1.3 Guidance cues**

The precise patterning of thalamocortical projection depends on intrinsic and extrinsic mechanisms, including the navigation of many extracellular molecules to the membrane receptors, thalamic neural activity, and the axonal interactions between thalamocortical and corticothalamic projections. Some guidance cues interact with proteins in the GC membrane, which direct the growth of thalamocortical fibers by regulating the organization of the cytoskeleton.

#### **Sema3A/L1**

Semaphorins and their receptors are regulators of repulsive axon guidance through the nervous system, where they are important for pathfinding and fasciculation of olfactory, spinal and cranial axons (Schwarz and Ruhrberg, 2010). It was reported that  $L1^{-/-}$  thalamocortical axons in mice were hyperfasciculated but normally target into the motor, somatosensory, and visual cortex (Ohyama et al., 2004). Wright *et al.* reported that thalamocortical axons of  $CHL1^{-/-}$  mice were not altered in fasciculation at the ventral telencephalon or cortex but showed misrouting of somatosensory projections. The proposed mechanism was that CHL1 as a coreceptor for Neuropilin1 to guide TCA projection because CHL1 interacted with Neuropilin1 through the Ig1-sequence FASNRL to mediate repulsive axon guidance to Sema3A (Wright et al., 2007). These receptors showed different thalamocortical projection although their functions were repulsive to Sema3A. These results suggested that axon guidance of nervous system was a very complex process. Those receptors were specifically expressed in several subpopulations of thalamic axons. Knock-out of one receptor would affect the expression other receptors. Further research showed that

L1 and CHL1 interact with EphA receptors and cooperated to guide subpopulations of thalamic axons to different cortical regions (Demyanenko et al., 2011).

### **Netrin/DCC (attractive)/UNC5 (repulsive)**

Several studies have revealed that netrin played an important role in thalamocortical projection. Braisted *et al* (2000) found that netrin-1<sup>-/-</sup> TCA projection was disorganized in the ventral telencephalon, and fewer dorsal thalamic axons reached cortex (Braisted et al., 2000). Attraction was exclusively mediated by netrin-1 binding to DCC. By contrast, repulsion might occur through two distinct mechanisms: short-range repulsion was desirable when netrin-1 bound to UNC5, or through the simultaneous binding of netrin-1 to UNC5 and DCC when long-range repulsion was required (Cirulli and Yebra, 2007).

Furthermore, an essential study from Bonnin *et al.* enhances the understanding of netrin in thalamocortical guidance. In the explant culture assays, axons originating from anterior and posterior halves of E14.5 dorsal thalamus respectively responded repulsive or attractive to netrin-1, reflecting the patterns of *DCC* and *Unc5c* expression. *Unc5c* expression formed a distinct rostral-high to caudal-low gradient throughout the ventrodorsal axis. Interestingly, *DCC* was expressed in a very slight anterior-low to the posterior-high gradient. At E16.5, *DCC* was expressed throughout the dorsal thalamus. Hence, the 5-HT receptor, which altered DCC/*Unc5c* ratio, converted the attraction exerted by netrin-1 on posterior TCAs to repulsion (Bonnin et al., 2007). That information showed that development of the TCA required the orchestrated execution of comprehensive genetic programmes, rather than the action of individual genes.

### **Slit/Robo**

Robo1 knockout mice displayed aberrant axonal pathfinding in the corpus callosum and the hippocampal commissure (Andrews et al., 2006). *Slit2* or *Slit1/2* double knockout mice showed thalamocortical pathfinding, which ventrally project and very few enter the CP. Unlike these two mutants, the TCA in Robo1 knockout mice reached their targets at least one day earlier than in control mice (Andrews et al., 2006; Blockus and Chedotal, 2014). Afterwards, it was shown that the guidance receptor Robo1 was upregulated by the decrease of spontaneous Ca<sup>2+</sup> activity when TCAs extended through the cortex. Shortly, Ca<sup>2+</sup>

spikes/*robo1* appeared to function as a brake for TCA growth (Mire et al., 2012). Therefore, the guidance cue Slits trigger the downstream signaling cascade by its receptors Robo.

The signaling pathways of those guidance cues were popularly reported (Guan et al., 2007; Hall and Lalli, 2010; Lowery and Van Vactor, 2009; Ming et al., 1997). On guidance cue stimulation, the receptor induces the assembly of signaling complexes within the GC, leading to activation of cytoskeleton regulators, like the GTPases Rac1 and RhoA. Interestingly, numerous studies suggest that both Sema3A and Netrin1 signaling recruit the effectors, members of Ezrin-Radixin-Moesin (ERM) complexes (Antoine-Bertrand et al., 2011; Deming et al., 2015; Mintz et al., 2008; Schlatter et al., 2008).

ERM are widely expressed proteins, which link the filamentous actin to the plasma membrane. They act as critical regulators in signaling transduction pathway to control the protrusion/retraction of the GC. When ERM proteins are in inactive forms, the highly conserved N termini, so called FERM domains, associate with their C termini. When the intramolecular interaction is removed, the ERM proteins transfer close and inactive forms into open and active state. The unmasked FERM bind directly or indirectly to membrane proteins, and their C-termini bind directly to actin (Bretscher et al., 2002; Ramesh, 2004).

CHL1 can recruit Erin, and this process requires a membrane-proximal motif (RGGKYSV) in the CHL1 cytoplasmic domain. This sequence in CHL1 is shown to be necessary for Sema3A-induced GC collapse and CHL1-dependent neurite outgrowth and branching in cortical embryonic neurons (Schlatter et al., 2008). Mintz *et al.* further confirmed that C-terminal deletion of Ezrin abolishes GC collapsed upon the stimulation of Sema3A. Meanwhile, Sema3A could affect active ERM redistribution (Mintz et al., 2008).

It has been demonstrated that netrin-1 induces the formation of an activated ERM/DCC complex in GC filopodia, which is required for netrin-1-dependent cortical axon outgrowth (Antoine-Bertrand et al., 2011). Netrin-1 regulates the interaction between DCC and Ezrin, and induces the phosphorylation of ERM. After adding Netrin-1 for 5mins, the peak level of pERM is shown in embryonic cortical neurons. Afterwards, it maintains in a decreased but a stable high level than the non-treated neurons. Two decades ago, it was shown that Netrin/DCC signaling activated cAMP/PKA. Inhibition or loss of cAMP/PKA signaling converted GC attraction of netrin into repulsion (Ming et al., 1997). Recent evidence



suggests that DCC, ezrin, and PKA form a complex, and ezrin serves as a DCC-associated PKA anchoring protein (Deming et al., 2015).

## 2 Materials and Methods

### 2.1 Mouse mutants and tamoxifen injection

To generate a conditional knockout allele (PRG-2<sup>fl<sup>ox</sup></sup>), a neomycin resistance cassette was introduced at the 3' end of exon 1 of PRG-2 gene. LoxP site flanked exon 1 and the neomycin resistance cassette. Upon Cre-mediated recombination, exon 1 and the neomycin resistance cassette were excised from the PRG-2 locus, resulting in a null allele. These mice were crossed to Deleter<sup>Cre</sup> to generate PRG-2<sup>-/-</sup> (coPRG-2<sup>-/-</sup>) mice lines (Schwenk et al., 1995).

Gbx2<sup>CreER</sup> mice were provided by J. Li (UConn Health Center). R26<sup>loxP-STOP-loxP-tdTomato</sup> (R26<sup>tdTomato</sup>) mice were purchased from Jackson laboratories (stock#007905). Genotyping for CreER was performed as described, and genotyping for the R26<sup>tdTomato</sup> allele was performed as described on the jax.org website. To inactivate PRG-2 in thalamic neurons, E12.5 pregnant PRG-2<sup>fl/fl</sup>/Gbx2<sup>CreER</sup>/R26<sup>tdTomato</sup> female mice were administrated 4 mg of tamoxifen (20 mg/ml in corn oil) by oral gavage as described (Brown et al., 2009). The vaginal plug was detected in the morning of the day, and was considered as embryonic day E0.5. All experiments on PRG-2 KO, Radixin KO mice (for details on genetic manipulation, breeding and genotyping see (Kikuchi et al., 2002)), backcrossed on a C57Bl/6J background for at least seven generations, and for PRG-2<sup>fl/fl</sup>/Gbx2<sup>CreER</sup>/R26<sup>tdTomato</sup> mice were conducted in accordance with the national laws for the use of animals in research and with the European Communities Council Directive 86/609/EEC, and the process were also approved by the local ethical committee (Landesuntersuchungsamt Rheinland-Pfalz 23. 177-07/G 13-1-073). Experiments were designed to minimize the number of animals used. Animals were sacrificed at different time-points.

### 2.2 Immunofluorescent stainings (IF)

Time-mated animals were anesthetized (0.5% ketamine i.p.) and transcardially perfused with 4% paraformaldehyde (PFA) for IF stainings. Brains were postfixed overnight in 4% PFA and further processed. Brains were sectioned by vibrating microtomes (Thermo Microm HM650V), and brain sections were blocked for 6hrs (10% normal goat serum and 0.2% Triton-X) before overnight incubation with primary antibodies at 4°C. Sections were finally immunostained with Alexa-labeled secondary antibodies (Alexa 488, Alexa 568 or Alexa 647,

all Invitrogen, Germany). Colocalization studies were performed using antibodies against PRG-2 (custom-made antibody against directed against the amino acid sequence 701-716 located in the C-terminal part of PRG-2; dilution: 1:6000), L1 (1:1000; MAB5272, Merck Millipore, USA), ATX (1:250, 3D1(Tanaka et al., 2004)), LPA (mAB LT3114, 1µg/ml, custom made antibody described in (Goldshmit et al., 2012)), GFP (1:1000; ab290, Abcam, UK), Tuj1(1:1000; MMS-435P, Covance, USA), Phalloidin (1:1000; A12379, Life Technologies, USA), Radixin (1:800; SC-6408, Santa Cruz, Germany), pERM (1:800; #3141, Cell Signaling, USA), CTFG (1:1000; sc-14939, Santa Cruz, USA), VGlut2 (1:1000; AB2251, Merck Millipore, USA ), NeuN (1:1000; MAB377, Merck Millipore, USA) and Ctip2 (1:1000; ab18465, Abcam, UK). Confocal images were obtained on a Leica SP8 equipped with standard lasers and a white light laser (WLL). Maximum intensity projection images used for display were produced using Leica confocal software. Stitched images were produced using Leica confocal software or Adobe Photoshop CS6. Linear alterations to original images were performed to enhance contrast and brightness.

### **2.3 Anterograde and retrograde tracing**

P5 mice were anesthetized (0.5% ketamine i.p.), transcardially perfused with 4% PFA and postfixed overnight in 4% PFA. NeuroVue®Jade(excitation: 478, emission: 508), Red (excitation: 567, emission:588) or maroon (excitation: 647, emission: 667, all from Polyscience, Inc., USA) was cutted into 0,5\*0,5\*1,5mm pieces, then inserted into the VB, Po, or cortex in mice brains. And incubate at 37°C for two months. For the embryonic brain staining, the lipophilic dye was inserted into the dorsal thalamus of overnight fixed brains.

### **2.4 Cytochrome oxidase staining**

After incubating in 30% sucrose overnight, the brains were cutted into 50-100 µm thick tangential sections and stained for cytochrome oxidase, which was processed in 0.06% cytochrome C (C2506, Sigma), 4.44% sucrose, 0.032% DAB (D5637, Sigma), 0.0008% Cobalt Chloride, 0.0007% Nickel Ammonium Sulfate and 0.46% catalase (Catalase from bovine liver, C100, Sigma) for 45 mins at 37°C. Depending on the axis of the cut, barrels sometimes spread over several slices (Tolner et al., 2012). Analysis of barrel surface was performed using ImageJ.

## **2.5 Slice culture, biocytin labeling and slice electroporation**

Organotypic slices were prepared from 300  $\mu\text{m}$  thickness brain slices along a 45° section plane (between sagittal and coronal) by Vibrating Microtome 5000 mz (Campden Instruments Ltd.), which encompass the trajectory of TCAs. Brain slices were cultured on Hydrophilic Polytetrafluoroethylene membranes (PICM0RG5 0.0.4 $\mu\text{m}$  pore size; Merck Millicell) in organ tissue dishes containing 1 ml of medium MEM (ref 41090-028, Gibco) supplemented with 33 mM glucose (Fresenius Kabi), 1.87 mM L-alanyl-glutamine, 10% FBS (lot:0227D, Merck), and 100 units penicillin/100  $\mu\text{g}$  streptavidin (15140-122, Gibco). After 3hrs incubation, the medium was changes to 1 ml of Neurobasal (ref 21103-049, Gibco) supplemented with 2% B-27 (ref 17504-044, Gibco), 52 mM glucose, 20 mM L-alanyl-glutamine and 100 units penicillin/100  $\mu\text{g}$  streptavidin.

For biocytin tracing experiments, Pressure injections were performed using glass capillaries (1B100F-4, WPI, Germany) attached to a Toohey Spritzer (Toohey Company, USA). Biocytin Alexa fluor® 488 or 596 (Thermo) was gently induced into the thalamic region of E17 embryonic brains. Slices were then incubated for 6hrs and fixed with 4% PFA.

For electroporation experiments, corresponding plasmids were injected into organotypic slices cultured on Hydrophilic Polytetrafluoroethylene membranes. Then the brain slices were electroporated by Needle Tungsten Electrode(nepagene CUY614T&CUY615) and NEPA21 Super Electroporator in Petridish (nepageneCUY701P5E) with fresh Krebs buffer (NaCl 0.126 M, KCl 2.5 mM,  $\text{NaH}_2\text{PO}_4$  1.2 mM,  $\text{MgCl}_2$  1.2 mM,  $\text{CaCl}_2$  2.5 mM, Glucose 11.1 mM and  $\text{NaHCO}_3$  25 mM). Following the poring pulse mode (99 V voltage, 1 ms pulse length, 50 ms pulse interval, 2 number of pulses, 10% decay rate), the transfer pulse mode was performed (40 V voltage, 5 ms pulse length, 500 ms pulse interval, 5 number of pulses, 40% decay rate with polarity switching).

## **2.6 Thalamic and cortical explants**

Embryonic brains were sliced by McIlwain tissue chopper or Vibrating Microtome. The 400\*400\*250  $\mu\text{m}$  tissue was put 300  $\mu\text{m}$  away from the LPA -coated 0.5\*0.2cm rectangle on the culture glass. The LPA region was composed by 10  $\mu\text{M}$  TF-LPA (TopFluorLyso PA, 810280, Avanti Polar Lipids, Inc), or 1  $\mu\text{M}$  LPA (BML-LP100-0025, Enzo) with fluorescence beads

(FluoSpheres® Carboxylate-Modified Microspheres, F8812, Thermo). Matrigel (356237, Corning) immediately covered both plated tissue and pre-coated LPA. After Matrigel was polymerized at 37°C for 10 mins, the explant was cultured in multiwell plates (Nunclon Delta Surface, 176740, Thermo) with 300 µl DMEM/F12 medium (21103-049, Gibco) supplemented with 17.5 mM glucose, 2.5 mM L-glutamine, 5% FBS (0227D, Merck), 2% B27 (17504, Gibco) and 15 units penicillin/15 µg streptavidin. After 40hrs incubation, the explants were fixed with 4% PFA and were blocked in 5% NGS and 0.2% Triton. For staining of thalamic axons, slices were incubated with an antibody against Tuj1 (1:1000, MMS-435P, Covance, USA), and were visualized with a secondary Alexa 488 or Alexa 568 goat anti-mouse antibody (1:000). Thalamic explants were imaged using a confocal laser microscope (Leica SP8 equipped with a white light laser). In order to avoid bias e.g. by a different positioning to the LPA-containing matrigel, axon numbers were counted 100µm in front of the 10 µM TF-LPA-containing matrigel and 100µm and 200µm beyond the border of the LPA-containing matrigel. The border of the 10µM TF-LPA-rich matrigel was delineated by its TF-LPA fluorescent label. This procedure allowed normalization of axon numbers in the LPA-containing matrigel for each thalamic explant avoiding bias which might arise from putative differences in manual positioning of the thalamic explants. The ability of WT and PRG-2<sup>-/-</sup> fibers entering a TF-LPA rich zone was then calculated as a percentage of total fibers which arrived at the region before 100 µm away from the LPA boundary. Furthermore, to assess the endogenous outgrowth capacity of the thalamic fibers, the number of fibers at the same distances from the explants border in the adjacent quadrant (which did not contain LPA) had been assessed and normalized these values in the same way as described above.

## **2.7 Preparation of hippocampic neuron culture**

Mouse hippocampal neurons were isolated from E17 embryos. The neurons were plated on the poly-L-lysine-coated glass coverslips (P1274, Sigma), and maintained with 1 ml of MEM medium (41090-028, Gibco) supplemented with 38 mM glucose, 1.87 mM L-alanyl-glutamine, 10% HS (16050-122, Gibco), and 100 units penicillin/100 µg streptavidin (Gibco) for 3hr. Afterwards, the medium was changed to 1 ml of serum-free Neurobasal (21103-049, Gibco) plus 2% B-27, 25mM glucose, 20 mM L-alanyl-glutamine and 100 units penicillin/100 µg

streptavidin. All cultures were maintained in the incubator in a humid condition at 37 °C with 5% CO<sub>2</sub>.

## **2.8 Live imaging of RDX distribution in the GC**

Mouse hippocampal neurons (either WT or PRG-2<sup>-/-</sup>) were transfected by Effectene Transfection Reagent (Qiagen) at 1 day *in vitro* (DIV1) using 0.5 µg pEGFP-N2-RDX or Lifeact-RFP (Riedl et al., 2008) plasmid per well. At DIV3, live imaging experiments were performed using an inverted TCS SP5 confocal microscope (Leica) equipped with a hybrid detector (HyD, Leica) and a 63 x oil objective in a 35 °C heated and humidified incubation chamber. The LPA-coated pipette tip (500 nM LPA in matrigel) was placed 40 µm away from the center of the GC at an angle of 45° with respect to the initial direction of axon extension. In order to avoid bleaching of RDX-GFP, a 488 nm Ar-laser scanning was performed every 7 min for the next 60 mins.

## **2.9 Analysis of pERM distribution in GC**

After DIV2, 1 µM LPA was added in culture medium of mouse hippocampal neurons for 20 mins. Neurons were subsequently fixed and stained as described (Brandt et al., 2007). After immunofluorescent staining and confocal imaging using a Leica SP8, pERM staining intensity in GCs was quantified using ImageJ. To differentiate between the signal adjacent to the membrane and the signal in the center of the GC, the GC contour was traced and applied the enlarge function of ImageJ using negative values to draw concentric contours towards the center of the GC at a distance of 1 µm. The ROI containing the area below the GC membrane was assigned as the periphery, and the area in the center of the GC was assigned as a center. The signal intensity was measured by ImageJ.

## **2.10 Analysis of pERM expression in dissociated neurons**

To assess the effect of LPA on ERM phosphorylation, DIV7 primary cortical (hippocampus) neurons derived from PRG-2<sup>-/-</sup> mice or littermate controls were prepared as described in section 2.7, incubated over time at 37 °C, 5% CO<sub>2</sub> and saturated humidity with different concentrations of LPA (Avanti Polar Lipids, Alabaster, AL) as indicated. The following steps were performed at 4 °C: cultured neurons were washed once in PBS, then harvested in lysis buffer which contained 1% (v/v) Triton-100, 2 mM EDTA, 1 mM PMSF (Applichem, Germany),

PhosSTOP phosphatases inhibitors (04906845001, Roche, Germany) and Complete proteases inhibitors (04693116001, Roche, Germany) in PBS. After incubation for 30 mins on ice, lysates were centrifuged at 1000 x g for 10 mins. The resulting supernatants were boiled in SDS sample buffer after adjustment of protein concentrations using a BCA assay (Pierce Biotechnology, USA). Samples were analyzed by western blotting (Hausrat et al., 2015).

### **2.11 Preparation thalamic neuron culture and GC collapse assay**

Mouse thalamic neurons were prepared from E14 embryos. The dissociated neurons were planted onto matrigel-coated glass coverlips maintained with the medium as the same as used in explant culture. The cells were used for collapse assay 15-20 hrs after plating. Juxtosomal pipettes with the tip inside diameter of about 0.5  $\mu\text{m}$  were pulled from 2mm filamented borosilicate glass. To assay GC collapse, the LPA-coated pipette (tip: 500 nM LPA in matrigel; inside, 500 nM LPA full of the pipette) was placed 40  $\mu\text{m}$  from the center of the growth cone of an isolated neuron and at an angle of 45° with respect to the initial direction of neurite extension. For the Sema3A collapse assay, 8  $\mu\text{g}/\text{ml}$  Sema3A was coated and put 20 $\mu\text{m}$  away. Microscopic images of neurites were captured with a CCD (charge-coupled device) camera (TKC1381; JVC, Yokohama, Japan) which attached to a phase-contrast microscope (CK-40, Olympus, Tokyo, Japan) and stored in a microcomputer for subsequent analysis using Scion Image programs. To determine the total length of neurite extension, the whole trajectory of the neurite at the end of the 1 hr period was measured with a digitizer. Only those GCs with a net extension of more than 5  $\mu\text{m}$  over the 1 hr period were included in the growth analysis (Yuan et al., 2003).

### **2.12 Quantitative PCR**

Total RNA from neocortex and thalamus tissue at different embryonic stages was extracted using the Aurum™ Total RNA Mini Kit (Bio-Rad). Quality and integrity of total RNA preparation was confirmed using a NanoDrop™ 2000c Spectrophotometer (Thermo Scientific). RNA was reverse transcribed into single-stranded cDNA using iScript™ cDNA Synthesis kit (Bio-Rad). QPCR was carried out on a CFX Connect™ Real Time Detection System (BioRad) using iScript™ One-Step RT-PCR Kit with SYBR Green (Bio-Rad). Each independent sample was assayed in duplicate and gene expression was normalized to that of Gapdh. For qPCR, the following set of primers were used: PRG-2 (forward

TGTCTACGTGTCGATGTACT and reverse ATRACTGGGTGATCTGTGTG); and Gapdh (forward TGGAGAAACCTGCCAAGTATG and reverse GAGTTGCTGTTGAAGTCGCA).

### **2.13 Statistics**

All data were analyzed using PRISM6 (Graphpad software). Data were presented as mean  $\pm$  SEM. All groups of the data were firstly assessed if Gaussian distribution or not. In two groups of data, nonparametric test were performed by Mann-Whitney *U* test. Statistical analysis of the parametric test for more than two groups was conducted using one-way ANOVA with Bonferroni correction. Otherwise, nonparametric test was analyzed by Kruskal-Wallis test with Dunn's multiple comparisons test. In analysis of contingency tables, Fisher's exact test was used. Asterisks indicated significance with \**P* < 0.05, \*\**P* < 0.01, \*\*\**P* < 0.001, \*\*\*\**P* < 0.0001 for all data sets.



## 3 Results

### 3.1 *PRG-2* is expressed in developing brains

*PRG-2* is prominently expressed in the thalamus (as shown by *in situ* hybridization in open source data base genpaint.org ID EB1482, see Figure 3.1A). Using real-time PCR, it was found that *PRG-2* mRNA levels in the mouse cerebral cortex gradually increases from E14 until postnatal day 1 (P1), after which levels decreased (Figure 3.1B). Compared to the cortex, the relatively high level of *PRG-2* mRNA in the thalamus remained stable from E14 when thalamic neurons started to project and decreased after P5.

*PRG-2* protein is distributed in the thalamocortical pathfinding from E13 in the developing mouse brains; it can be detected in TCAs as exemplarily shown at E18 by immunostaining (Figure 3.2A). Most of *PRG-2* TCAs are present in the IZ when they arrive at the neocortex. Few TCAs start to innervate into CP before E18. Until given birth, these fibers sprint to integrate into cortical circuits. Neural cell adhesion molecule L1, a marker for TCAs plays a major role in the development of TCAs. Axonal tracing experiments showed that L1-deficient TCAs were abnormally and highly fasciculated when they pass through the developing internal capsule (Ohyama et al., 2004). Here, it was shown that *PRG-2* and L1 both as membrane proteins co-localized in these TCA (Figure 3.2C and 3.2D). However, both of them had no distribution in the nucleus of thalamic neurons (Figure 3.2G). Furthermore, when anti-*PRG-2* antibody was also used in *PRG-2*<sup>-/-</sup> brains, no signal was detected in the whole brain slice (Figure 3.2B, 3.2E, 3.2F and 3.2H).

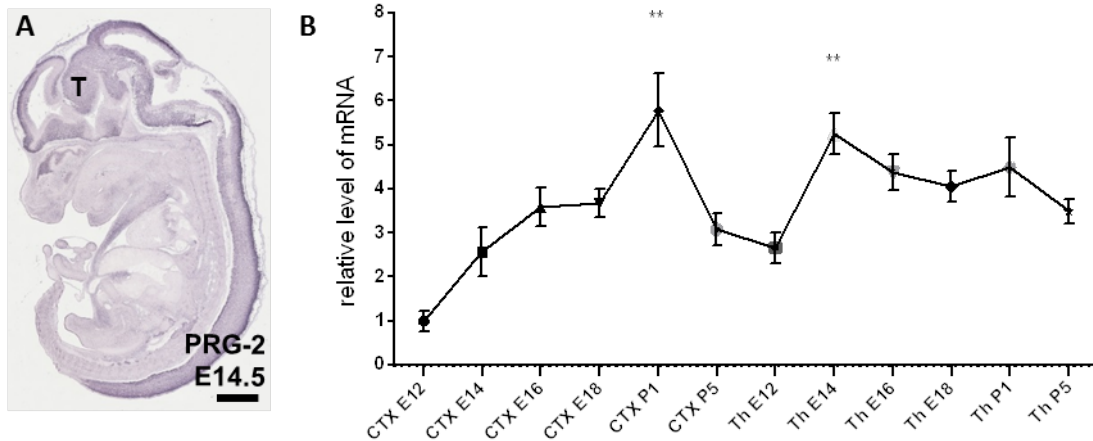


Figure 3.1 *PRG-2* mRNA is expressed in the mouse embryonic brains

(A) Distribution of *PRG-2* mRNA in mouse E14.5 brain by *in situ* hybridization (genpaint.org ID EB1482)

(B) *PRG-2* mRNA expression profiles at different stages in neocortex or S1 cortex and thalamus by real-time (RT)-qPCR analysis. (Kruskal-Wallis (K-W) test with Dunn's Multiple Comparison Test,  $P=0.0026$  )

\*\* $p < 0.01$ . Bars represent mean  $\pm$  SEM. Scale bar represents 900  $\mu\text{m}$ .

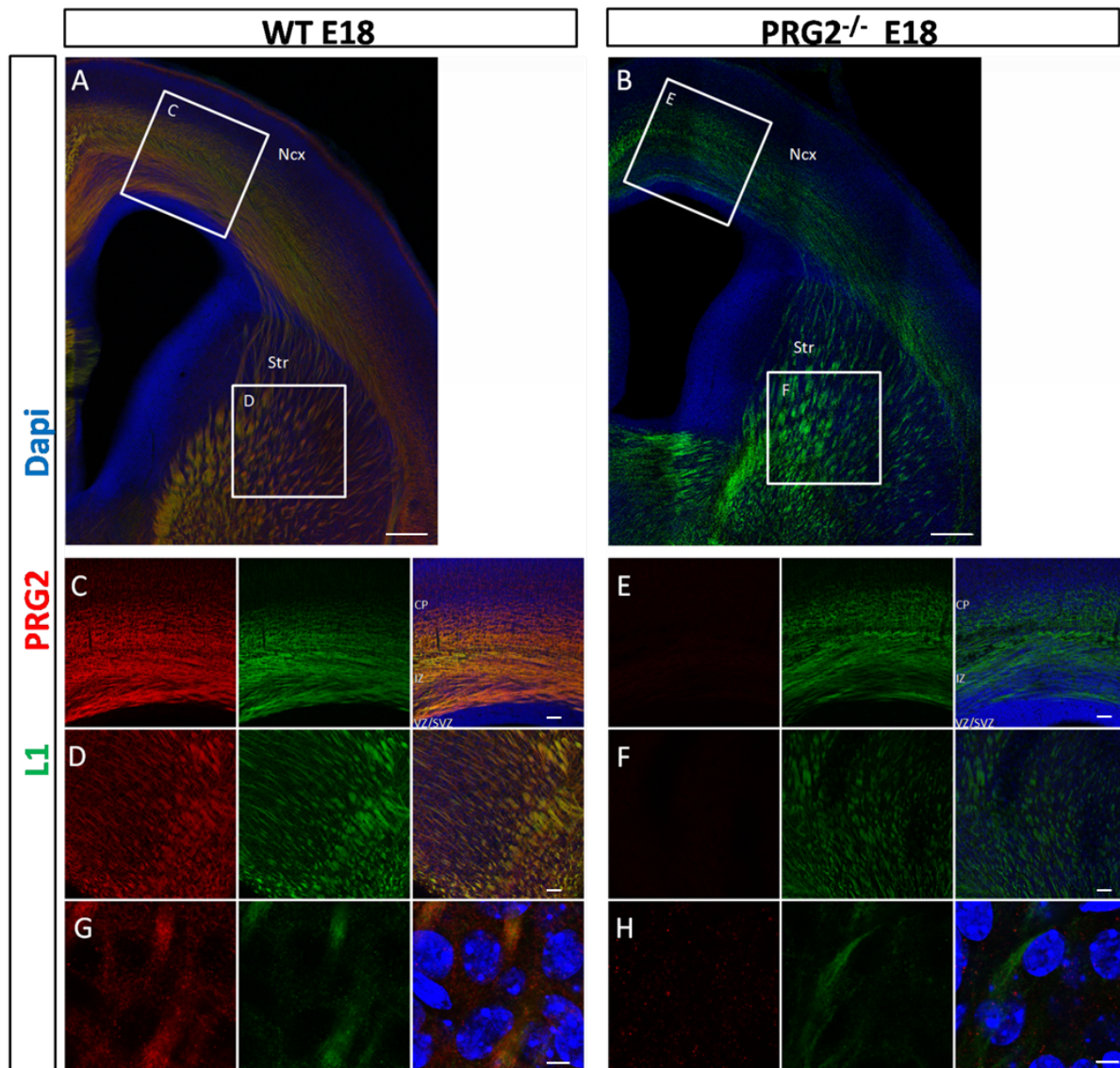


Figure 3.2 PRG-2 protein is expressed in thalamocortical fibers

(A-B) PRG-2 is expressed in the forebrain and co-localizes with the axonal marker L1 at E18 of WT (A), but it is not expressed in PRG-2<sup>-/-</sup> (B).

(C-H) PRG-2 and L1 expression in the cortex(C and E), internal capsule (D and F) and thalamus (G and H) of WT and PRG-2<sup>-/-</sup> slices.

Scale bars represent 200  $\mu$ m (A and B), 50  $\mu$ m (C-F), 5  $\mu$ m (G and H).

### 3.2 PRG-2 knock-out mice have a defect in thalamocortical projection

According to PRG-2 expression pattern, it is hypothesized that PRG2 has an important role in the developing thalamocortical projection. Hence, anterograde tracing was performed by inserting the lipophilic dye NeuroVue in E17 thalamus of PFA-fixed brains. According to the dye diffusion, thalamocortical projections became visible. While thalamocortical fibers formed well-defined projections in the IZ in E17 WT animals (Figure 3.3A), thalamocortical fibers in PRG-2<sup>-/-</sup> mice were not restricted to IZ (Figure 3.3B), but invaded the CP.

To assess the functional outcome of altered thalamocortical projection in postnatal brains, the barrel cortex of P3-P5 WT and PRG-2<sup>-/-</sup> brains were analyzed. Barrels were not yet visible in P3 WT and PRG-2<sup>-/-</sup> mice except one obscure control (Figure 3.4A and 3.4B). However, all P4 WT barrels were visible (Figure 3.4C). In comparison, the appearance of barrels was delayed in 5 PRG-2<sup>-/-</sup> mice out of total 22 (Figure 3.4D and 3.4G). Both WT and mutant P5 mice showed mature cortical barrels (Figure 3.4E and 3.4F). In line, Vglut2 and NeuN antibody staining revealed that PRG-2<sup>-/-</sup> mice had a normal synaptic connectivity in P10 and P23 cortical barrels (Figure 3.4H-3.4K).

Since thalamocortical projection defects observed at prenatal stages might be a temporary feature that eventually disappears after formation of thalamocortical connections, the thalamocortical fiber tract at P5 was analyzed, a time point at which the connections of these fibers were established (Molnar et al., 1998). According to the discovery that a specific barreloid of VB neurons connected with a corresponding barrel of layer IV neurons (Pouchelon et al., 2012), NeuroVue was inserted into P5 ventrobasal thalamic nuclei (VB) and diffused to layer IV in the cortex. Hence, the thalamic projection could be visualized. As the tangential slices from layer IV were shown in Figure 3.5A and 3.5C, dye-stained WT axons were restricted to their corresponding barrels. However, in PRG-2<sup>-/-</sup> mice, thalamic axons readily crossed barrel borders aberrantly invading neighboring barrels (Figure 3.5B and 3.5D). To further assess misrouting in PRG-2<sup>-/-</sup> mice, I performed coronal slice cutting from these traced brains. As shown in Figure 3.5E, WT thalamocortical projection was restricted to its corresponding cortical column, while PRG-2 deficient fibers invaded the adjacent column

(Figure 3.5F). Thus, PRG-2 depletion in mice leads to a misrouting of thalamocortical projections.

To rule out other possible factors that could induce mistargeting of thalamocortical fibers, like defects in the corticothalamic projection and cortical layer defects, several experiments as follow were performed. Firstly, corticothalamic axons were traced by inserting different NeuroVue into different cortex area of P5 brains (Figure 3.6A and 3.6A'). WT (Figure 3.6B and 3.6C) and PRG-2<sup>-/-</sup> (Figure 3.6D and 3.6E) corticothalamic axons both target into the right region of thalamus, from Visual cortex to LGN, S1 to VB/PO and motor cortex to VA/VL.

Secondly, the antibody of cortical layer V marker Ctip2 was applied to P10 S1 cortex. According to the distribution of Layer V neurons, there was no obvious defect from cortical layer between WT (Figure 3.7A and 3.7A') and PRG-2<sup>-/-</sup> (Figure 3.7B and 3.7B'). Furthermore, cresyl violet staining of P23 also confirmed that no layers shift in the PRG-2<sup>-/-</sup> mice (Figure 3.7C, 3.7C', 3.7D and 3.7D'). Those data gave the hint that the deficient thalamocortical projections in PRG-2<sup>-/-</sup> mice resulted from the thalamocortical axon itself, not the cortex.

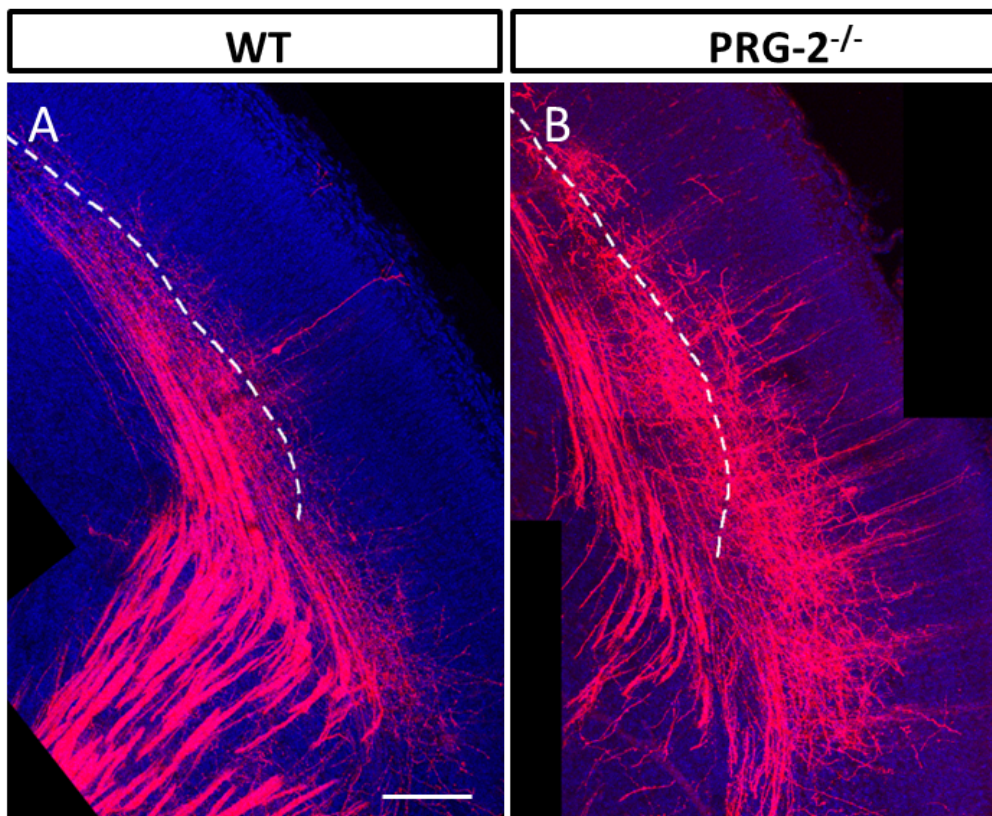


Figure 3.3 PRG-2 deficiency alters thalamocortical projections

(A-B) Anterograde fibers tracing using NeuroVue in E17 WT (A) and PRG-2<sup>-/-</sup> (B) delineated the TCAs. In control slice, thalamocortical fibers formed projections in the IZ. In PRG-2<sup>-/-</sup> mice, thalamocortical fibers were not restricted to IZ, but invaded the CP.

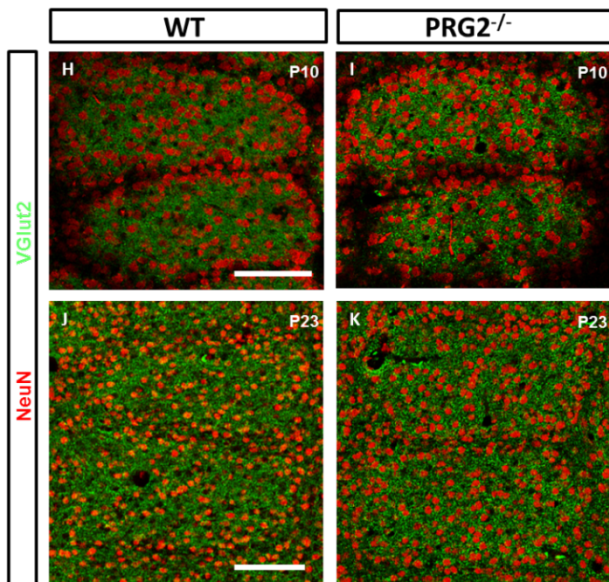
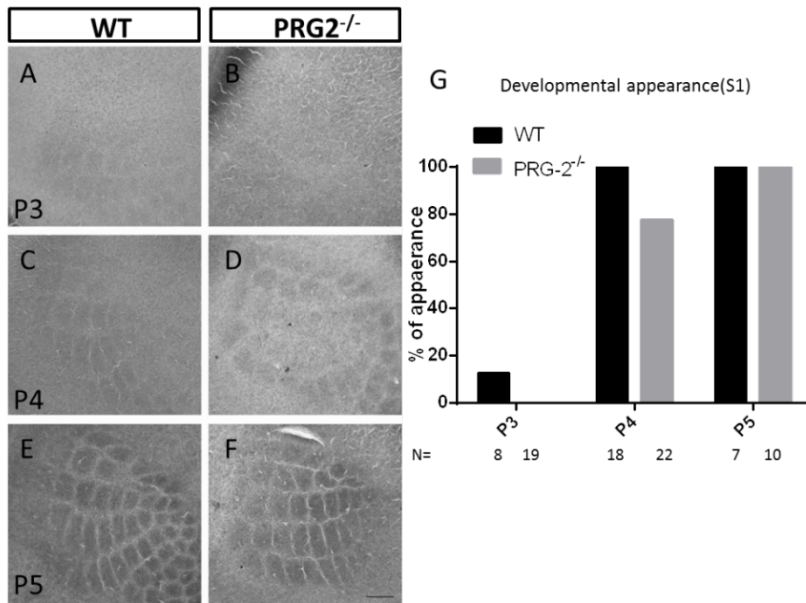


Figure 3.4 Developmental appearance of cortical barrels is slightly delayed in PRG-2<sup>-/-</sup> mice.

(A–F) Cytochrome oxidase histochemistry on flattened cortical sections at P3 (A and B), P4 (C and D), and P7 (E and F).

(G) Bar graph representing 1 day delay of barrel appearance in PRG-2<sup>-/-</sup> mice before P5. The number of mice examined is listed below.

(H–K) Synaptogenesis in cortical barrels of WT and PRG-2<sup>-/-</sup> animals at P10 (H and I) and P23 (J and K).

Scale bars represent 200 μm (A–F), 100 μm (H–K)

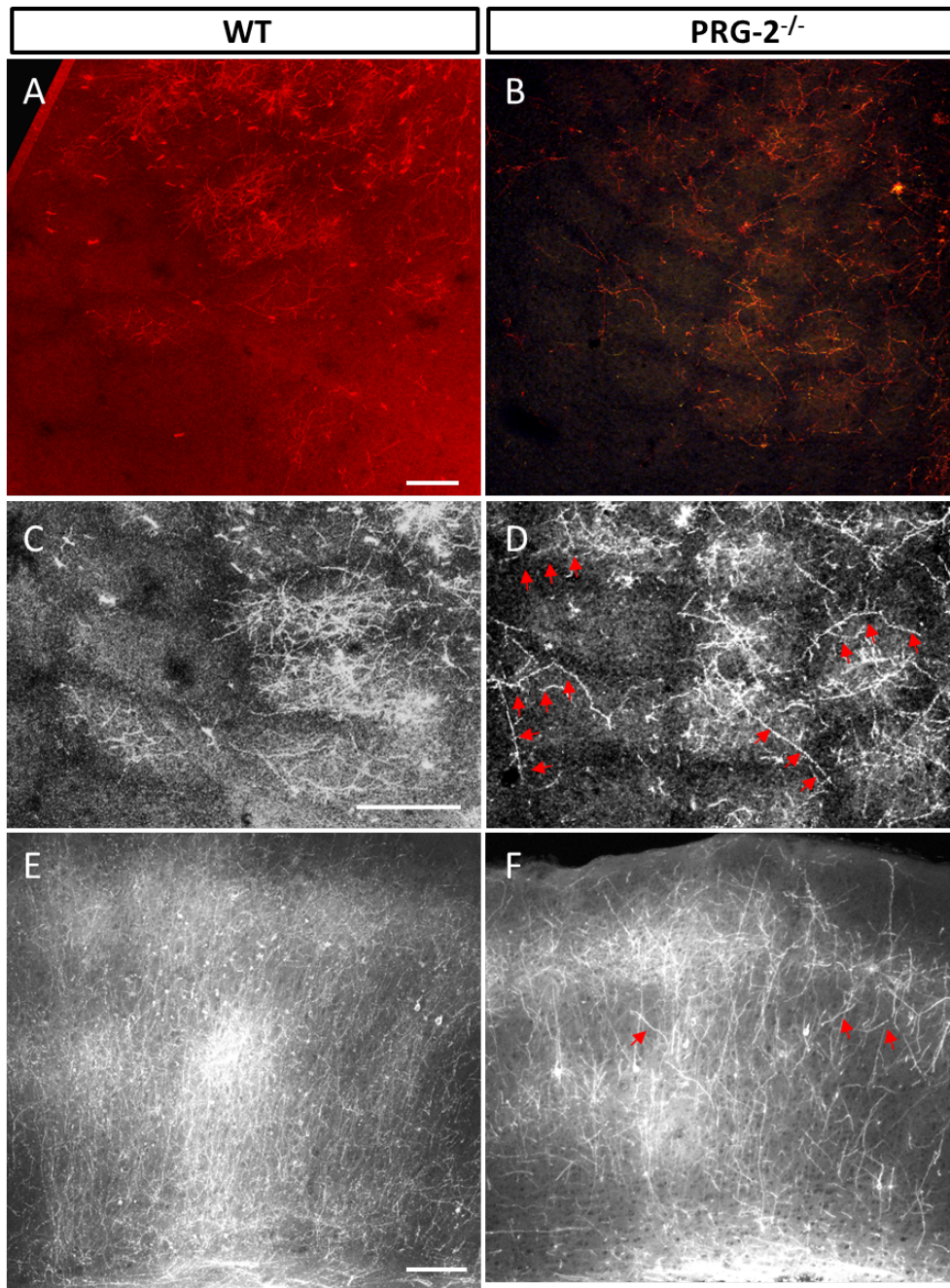


Figure 3.5 PRG-2 affects the TCAs en route to the target in the cortex at P5

(A–F) Anterograde TCAs tracing labeled by NeuroVue in the P5 VB of WT (A, C and E) and PRG-2<sup>-/-</sup> (B, D and F) brains. According to the tangential slices (A-D) and coronal sections (E and F), the PRG-2 deficient fibers invade the neighboring barrels.

Scale bars represent 100  $\mu$ m (A and F)



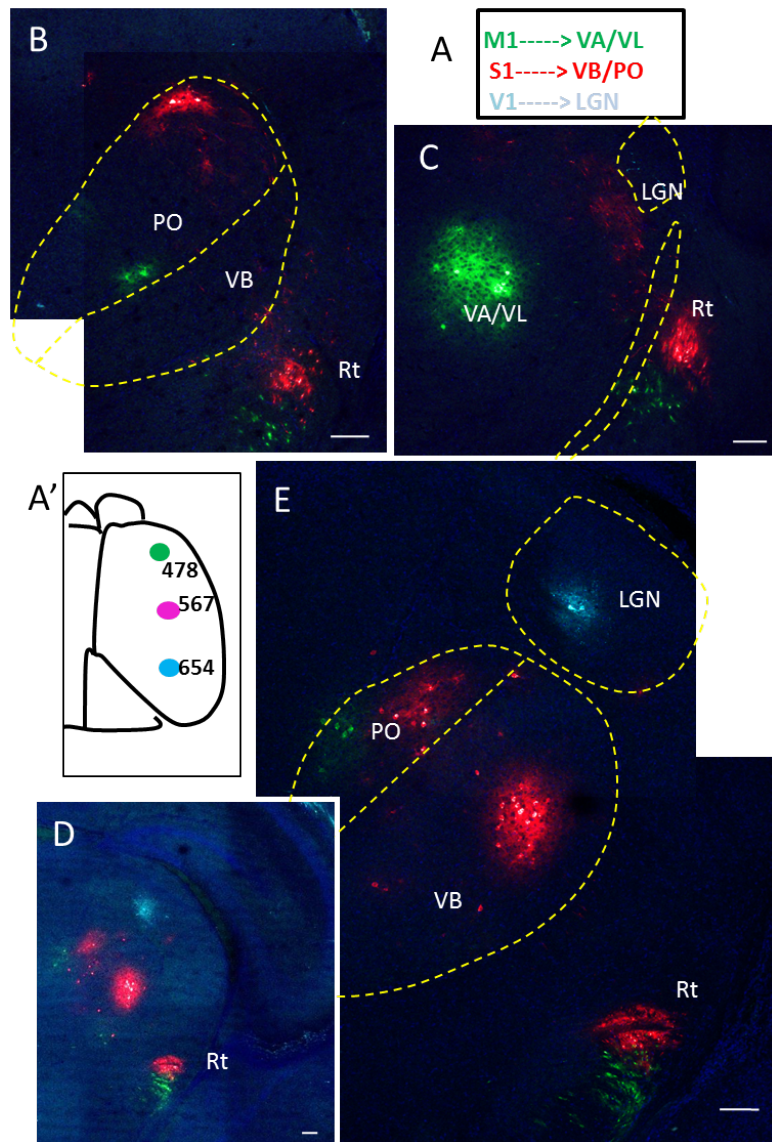


Figure 3.6 PRG-2 does not alter the corticothalamic axon route to the certain target in thalamus

(A and A'). Schematic overview of the NeuroVue tracer application in the motor cortex (NeuroVue Jade, 478nm), somatosensory cortex (NeuroVue Red, 567nm) and visual cortex (NeuroVue Maroon, 647nm).

WT (B and C) and PRG-2<sup>-/-</sup> (D and E) corticothalamic axons from particular cortical areas cross reticular thalamic nuclei (Rt), and display a grossly normal organization to thalamic nuclei.

Scale bars represent 100µm (B-E).

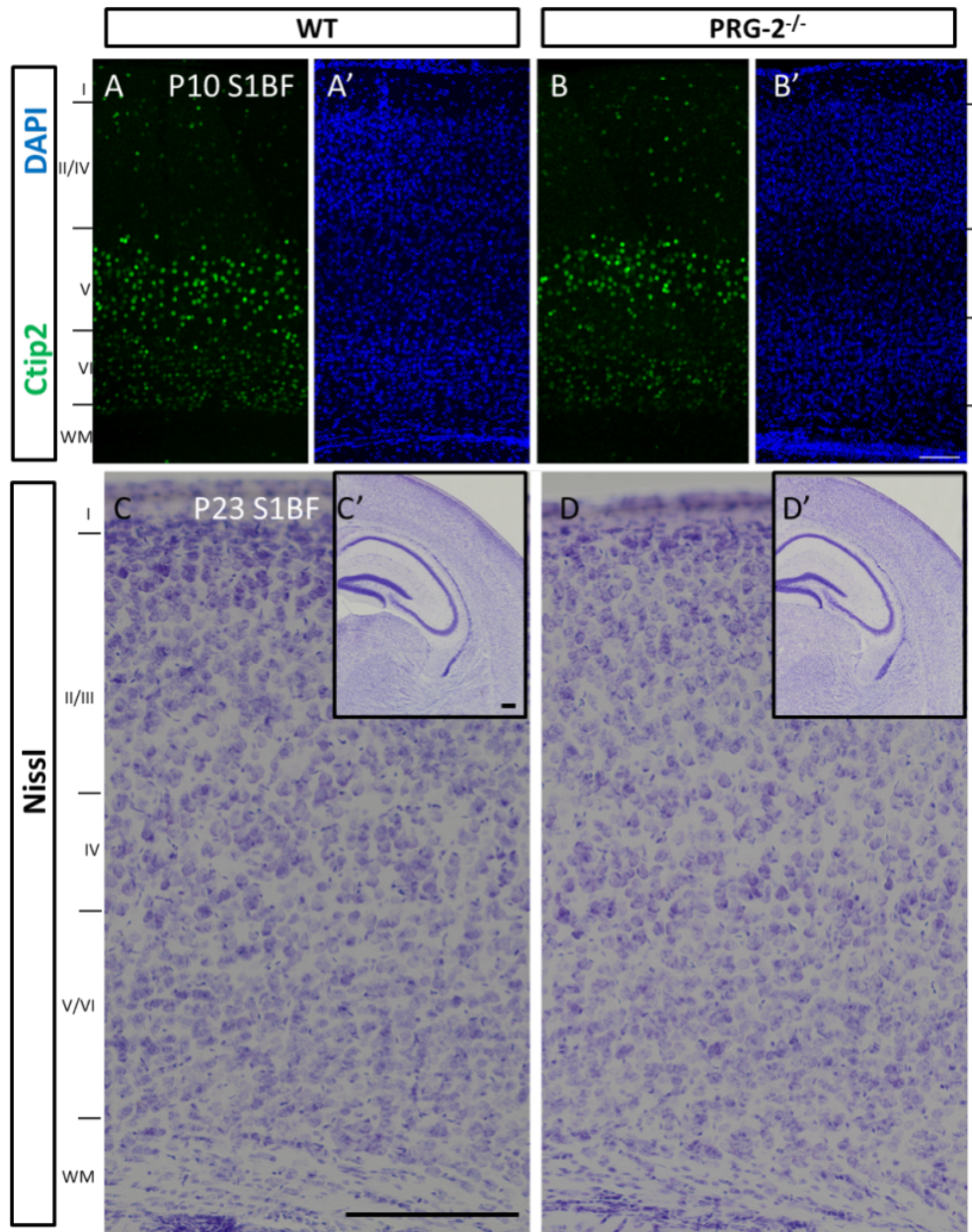


Figure 3.7 PRG-2 does not affect the distribution of cortical neurons

(A and B) Distribution of Layer V neurons labeled by layer V marker Ctip2 in P10 WT (A) and PRG-2<sup>-/-</sup> (B) S1 cortex.

(C and D) Nissl staining of P23 WT (C) and PRG-2<sup>-/-</sup> (D) brains at S1 cortex

Scale bars represent 100μm (A and B), 200μm (C and D).

### 3.3 PRG-2 is functionally required in thalamocortical afferents for correct targeting

To test whether the aberrant thalamic projection in PRG-2<sup>-/-</sup> mice was the result of the absence of PRG-2 from thalamocortical axons, brain slices cultures from E15 WT and PRG-2<sup>-/-</sup> mice were used, when it is at the peak of thalamocortical outgrowth. To visualize the thalamocortical projection, a GFP or PRG-2-expressing construct was electroporated into the ventrobasal part of the thalamus at E15.5. After 48 hrs, the slice cultures were fixed and fluorescent images were acquired to analyze the axonal projection (Figure 3.8A). After crossing the PSPB, the PRG-2 positive thalamocortical projection was restricted to the IZ avoiding the CP (Figure 3.8B and 3.8C; n = 11 slices), exhibiting a typical routine as shown in dye-traced slices (Figure 3.3A). In contrast, PRG-2<sup>-/-</sup> TCAs aberrantly invaded the CP (Figure 3.8D and 3.8E; n = 18 slices). However, when exogenous PRG-2 (PRG-2-IRES-GFP) was re-expressed in TCAs by electroporation, these fibers (delineated by additional GFP-expression) were again restricted to the IZ and did not show obvious differences to WT thalamocortical fibers (Figure 3.8F; n = 12 slices). When these rescued slices were resliced and stained by PRG-2 antibody, exogenous PRG-2 protein can be detected (Figure 3.8G). Quantitative analysis of thalamocortical cultures confirmed the significant amount of aberrant thalamocortical projections and the restoration of these axons after PRG-2 re-expression to WT levels (Figure 3.8H). It could be concluded that re-expression of PRG-2 in TCAs was sufficient to completely abrogate aberrant targeting of the thalamocortical fiber projection in PRG-2<sup>-/-</sup> slices.

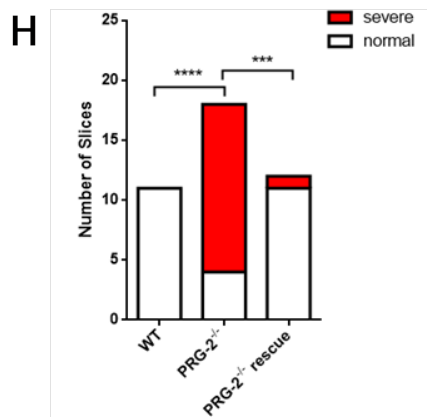
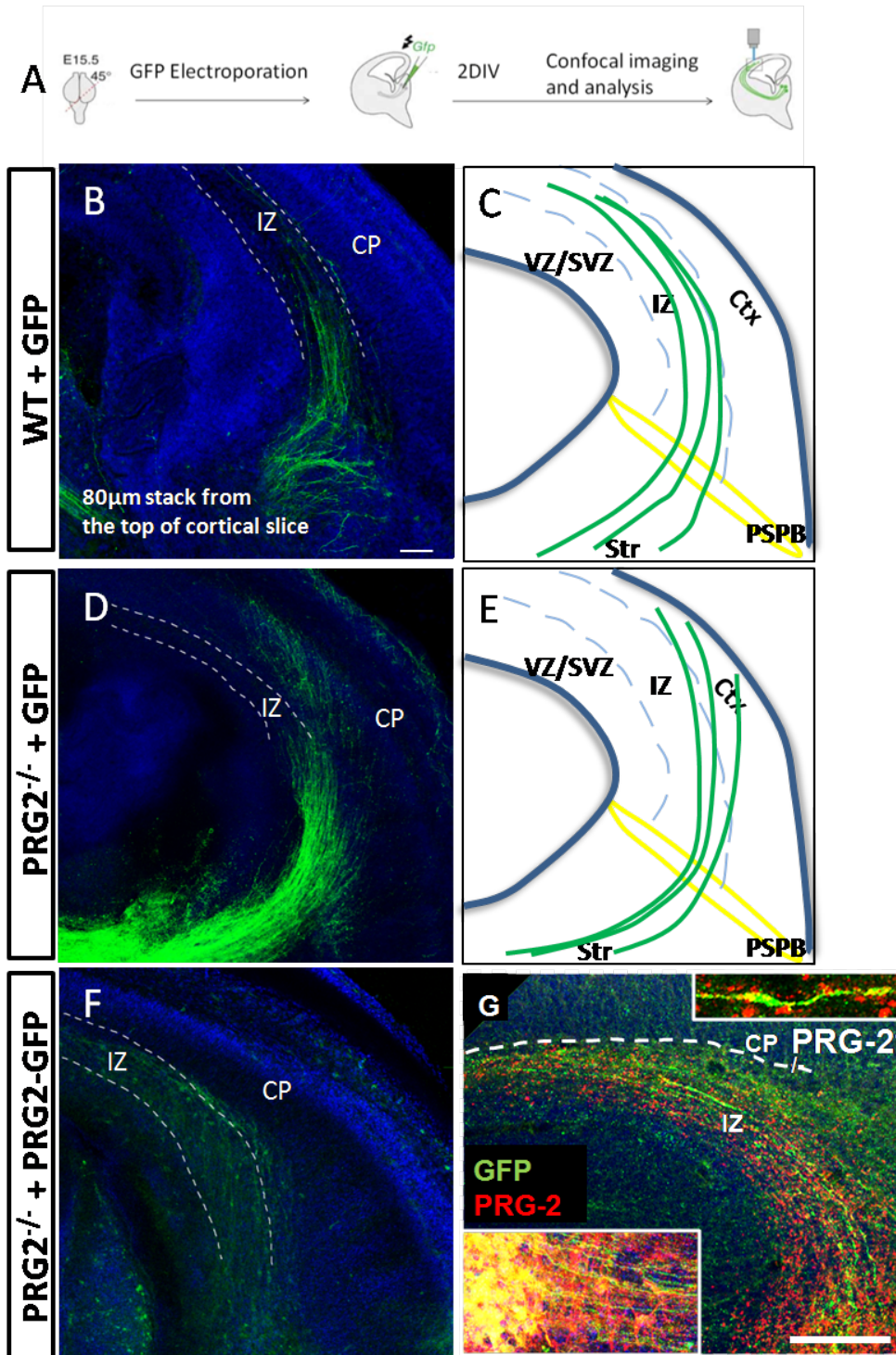


Figure 3.8 PRG-2 reconstitution rescues PRG-2<sup>-/-</sup> phenotype

(A) Schematic drawing of the thalamocortical slices preparation, GFP/PRG-2 electroporation and incubation time. Using a cutting angle of 45 degrees, thalamic neurons and their cortical projection region are maintained in a single slice.

(B and C) WT thalamocortical slice cultures transfected with GFP at E15.5 display a typical thalamocortical projection.

(D and E) In contrast, in PRG-2<sup>-/-</sup> thalamocortical slice cultures, aberrant fibers prematurely enter the CP.

(F) Re-expression of PRG-2 in PRG-2<sup>-/-</sup> slices from the same litter rescues the aberrant phenotype, resulting in the TCAs confined to the IZ (G).

(H) Statistical analysis reveal a significant aberrant thalamocortical projection in slices from PRG-2<sup>-/-</sup> mice those are restored to WT levels by PRG-2 re-expression (Fisher's exact test; number of analyzed slices = 11 WT, 18 PRG-2<sup>-/-</sup>, and 10 PRG-2<sup>-/-</sup> with PRG-2 re-expression).

\*\*\*p < 0.001, \*\*\*\*p < 0.0001. Scale bars represent 100μm (B, D, F and G)

### 3.4 Thalamus-specific PRG-2 knock-out mice have a defect in the thalamocortical projection

Cell-type-specific Cre driver lines, together with transgenic lines allow neuronal connectivity to be traced with cellular resolution. To temporally and spatially control *PRG-2* gene deletion, PRG-2<sup>fl/fl</sup>/Gbx2<sup>CreER</sup>/R26<sup>tdTomato</sup> (PRG-2<sup>ΔE12/ΔE12</sup>) mouse line was used to produce thalamus-specific PRG-2 knock-out mice with red fluorescent protein (RFP) as a reporter expressed in the whole thalamocortical projection. Tamoxifen was administered by oral gavage to timed-pregnant females at E12.5 (Brown et al., 2009; Normand et al., 2013), which provided temporal control of Cre<sup>ER</sup> release and subsequent translocation to the nucleus removing the Stop cassette from the reporter and exon1 of PRG-2 in PRG-2<sup>fl/fl</sup> mice.

*Gbx2* is expressed at early stages of dorsal thalamus development. Because *Gbx2* is not expressed in the cortex, it is likely that intrinsic properties of the corticothalamic fibers will be normal. Therefore, Gbx2<sup>CreER</sup> mouse line provides a useful experimental system to trace thalamocortical fibers. To validate the fidelity of PRG-2<sup>fl</sup> recombination in the thalamus, E18.5 PRG-2<sup>fl/fl</sup>/Gbx2<sup>CreER</sup>/R26<sup>tdTomato</sup> brain sections were analyzed by immunohistochemistry (IHC) using an anti-PRG-2 antibody. PRG-2 signal was weak in the RFP fibers near reticular thalamic nucleus (RTN) (Figure 3.9B-3.9D), so PRG-2-positive signal was mainly from corticofugal projections. The staining of fibers in internal capsule (IC) further confirmed the result. As shown in Figure 3.9E and 3.9F, PRG-2 positive corticofugal and tdTomato-stained thalamocortical projections connected and crossed together as described in the 'handshake' hypothesis, but there was no co-localization of PRG-2 with PRG-2<sup>ΔE12/ΔE12</sup> fibers expressing RFP. In fact, this accorded with earlier observations (Normand et al., 2013), which verified that Gbx2<sup>CreER</sup>-tamoxifen system was sufficient to make an efficient thalamus-specific knock out model.

To verify that the misrouted thalamocortical projection resulted from thalamus-specific PRG-2 knock-out, the Tdtomato-stained thalamocortical projections of E16 PRG-2<sup>+/+</sup>/Gbx2<sup>CreER</sup>/R26<sup>tdTomato</sup> and PRG-2<sup>fl/fl</sup>/Gbx2<sup>CreER</sup>/R26<sup>tdTomato</sup> brains were analyzed. Figure 3.9G and 3.9H presented the distribution of the entire thalamocortical projections in the

neocortex. Unlike WT fibers kept in the IZ (Figure 3.9G), PRG-2 deficient fibers had already invaded the lower CP (Figure 3.9H).

Furthermore, Alexa 488-biocytin tracing was injected in the VB of cultured thalamocortical brain slices of WT, PRG-2<sup>-/-</sup> and PRG-2<sup>fl/fl</sup>/Gbx2<sup>CreER</sup>/R26<sup>tdTomato</sup> mice at E17 (Figure 3.10A-3.10C), a time-point when TCAs accumulate below the subplate (Molnar et al., 1998). After the fluorescent biocytin uptake in thalamic neurons, the dye transported anterogradely from the soma to the growing fibers during 6 hrs incubation. While in WT slices thalamocortical fibers were restricted to the IZ (Figure 10A; n = 8 WT slices), as described by others (Molnar et al., 1998), in PRG-2<sup>-/-</sup> slices these fibers extended beyond the IZ and aberrantly protruded into the CP (Figure 3.10B; n = 13 slices). Quantitative assessment of these slices revealed a significant disruption of the thalamocortical projection in PRG-2<sup>-/-</sup> mice (Figure 3.10E). The result confirmed my previous findings in NeuroVue and electroporation slice tracing.

In parallel, PRG-2<sup>fl/fl</sup>/Gbx2<sup>CreER</sup>/R26<sup>tdTomato</sup> tracts showed a similar misrouting as it was observed in PRG-2<sup>-/-</sup> thalamocortical slices (Figure 3.10C; n = 14 slices). The Chi-square test showed significant difference between the WT and thalamic-specific PRG-2 knock-out slices (Figure 3.10E). Meanwhile, RFP upon cre-mediated recombination in thalamocortical fibers made the major thalamocortical fibers visible. As shown in Figure 3.10D, the RFP- fibers tended to innervate into cortical plate directly after crossing the PSPB.

The biocytin tracing in PRG-2<sup>ΔE12/ΔE12</sup> slice presented that not only a fiber subpopulation but the full thalamocortical projection aberrantly protruded into the CP. The thalamus-specific PRG-2 knock-out slices showed the same phenotype as the constitutive PRG-2<sup>-/-</sup>, which further confirmed that PRG-2 expressed in thalamic neurons played a critical role in thalamocortical development.

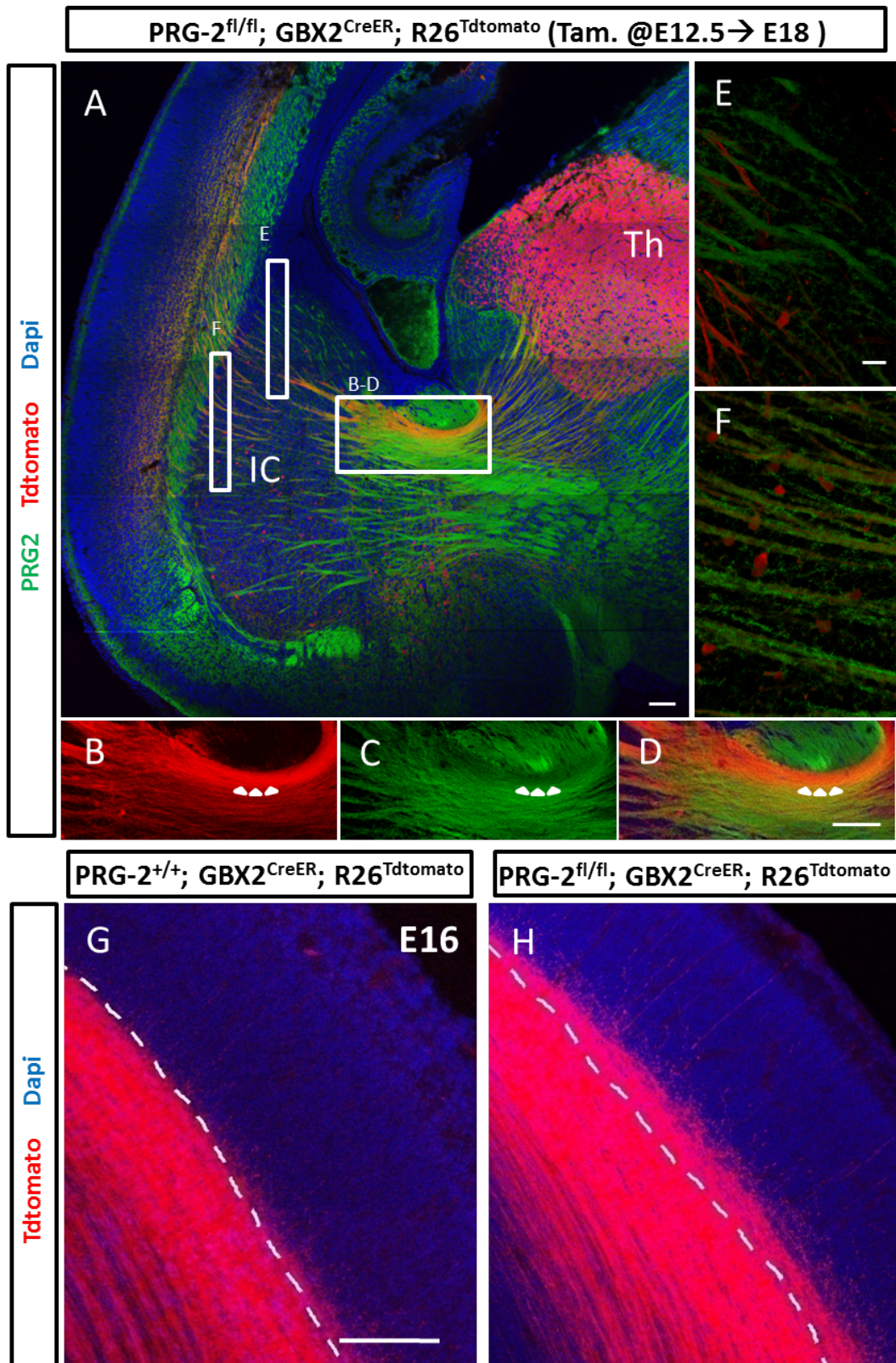


Figure 3.9 Thalamus-specific PRG-2 knock-out mice have a defect in thalamocortical projection



(A-F) Thalamocortical projection in PRG-2<sup>fl/fl</sup>/Gbx2<sup>CreER</sup>/R26<sup>tdTomato</sup> mice treated with tamoxifen at E12.5 (PRG-2<sup>ΔE12/ΔE12</sup>) is clearly visible by the R26<sup>tdTomato</sup> reporter expressing RFP. The overview picture (A) shows the strong RFP-signal in the thalamus (Th). When the TCAs cross the DTB, they accumulate into a bunch which express less PRG-2 (B-D). PRG-2 expressed corticothalamic axons don't co-localize with RFP-TCAs in IC (E and F).

(G-H) E16 PRG-2<sup>+/+</sup>/Gbx2<sup>CreER</sup>/R26<sup>tdTomato</sup> and PRG-2<sup>fl/fl</sup>/Gbx2<sup>CreER</sup>/R26<sup>tdTomato</sup> slices present the distribution of the entire WT thalamocortical projections maintain in the IZ (G), while PRG-2 deficient ones already have innervated into the lower CP (H).

Scale bar represents 100 μm (A-D, G and H) and 20 μm (E and F)

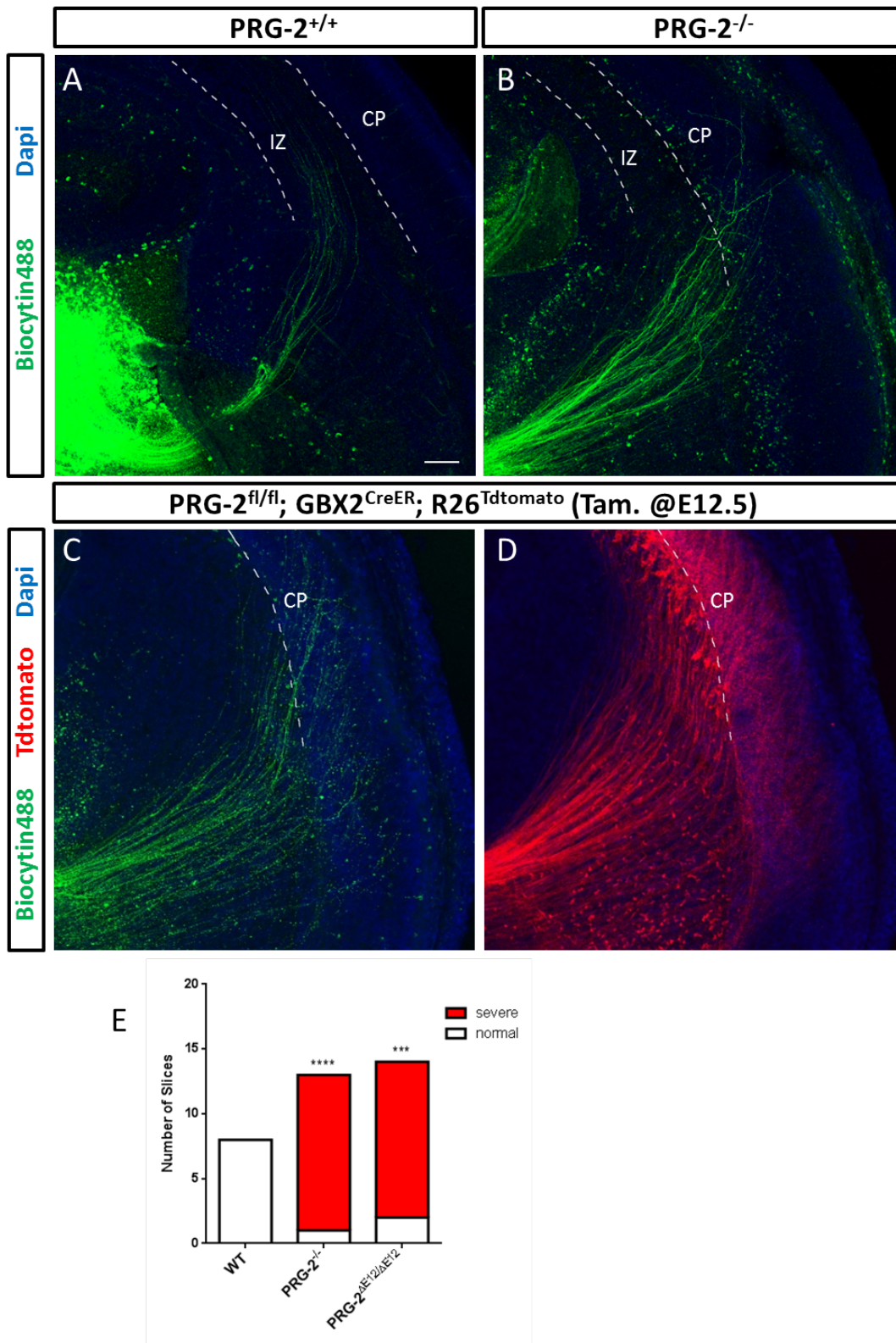


Figure 3.10 Biocytin 488 tracing *in vitro* confirmed the TCAs mispathfinding in PRG-2 knockout and PRG-2<sup>ΔE12/ΔE12</sup> mice

(A-D) Thalamocortical fiber tracing using biocytin injection in the ventrobasal (VB) nuclei of acute thalamocortical slices. While thalamocortical fibers of WT slices (A) are restricted to the IZ, thalamic axons of PRG-2<sup>-/-</sup> (B) and PRG-2<sup>ΔE12/ΔE12</sup> (C) slices aberrantly invade the CP. Specially, the RFP-labeled TCAs provide an intact misrouted projections in PRG-2<sup>ΔE12/ΔE12</sup> (D). (E) Quantitative analysis shows a significant amount of aberrant fibers in PRG-2<sup>-/-</sup> and in PRG-2<sup>ΔE12/ΔE12</sup> slices (Fisher's exact test; n = 8 WT, 13 PRG-2<sup>-/-</sup>, and 14 PRG-2<sup>ΔE12/ΔE12</sup> slices). \*\*\*p < 0.001, \*\*\*\*p < 0.0001. Scale bars represent 100 μm (A-D)

### 3.5 LPA signaling is critical for TCAs guidance in PRG-2<sup>-/-</sup> mice

Since PRG-2 is a member of the family of LPA-interacting molecules (Trimbuch et al., 2009), the expression of ATX, the LPA-synthesizing enzyme, was analyzed in the somatosensory cortex at E16. IHC results presented the strong ATX expression at the border of the CP and the intermediate zone (Figure 3.11A). This finding was in accordance with other studies, in which ATX was expressed by subplate neurons as shown on the mRNA level (Hoerder-Suabedissen et al., 2013).

Meanwhile, ATX expression overlapped with LPA and PRG-2, which was presented in fasciculated thalamocortical fibers (Figure 3.11B-3.11D). Whereas ATX and LPA expression was strong in the IZ as well as in the lower CP, almost no PRG-2 was expressed in the CP at E16 (Figure 3.11E-3.11H). These findings were consistent with a putative role of ATX/LPA in restricting PRG-2-expressing thalamocortical fibers to the IZ. Hence, the role of LPA synthesis was analyzed in the correct targeting of TCAs.

A recently characterized ATX blocker (0.1  $\mu$ M PF8380) (Gierse et al., 2010) was treated into the culture medium of E15 WT thalamocortical slices for 24 hrs. Subsequently, thalamocortical fibers of those slices were traced using biocytin and incubated for 12 hrs. WT thalamocortical fibers aberrantly invaded the CP by inhibiting ATX (Figure 3.12B), which was a similar phenotype also observed in slices from PRG-2<sup>-/-</sup> mice (Figure 3.3B). Quantitative analysis revealed that this phenotype was observed in 92% of all PF8380 treated slices (Figure 3.10E). To further study whether LPA from cortex induced this defect, 1.5  $\mu$ M PF8380 was injected locally into the CP at the beginning of slice incubation and after 24 hrs (Figure 3.12F). As shown in Figure 3.12C, inhibition of ATX in the CP was sufficient to induce an aberrant targeting of thalamocortical fibers, which was reminiscent of the phenotype observed in PRG-2<sup>-/-</sup> slices. Another inhibition experiment was also performed to identify other LPA source which could affect the TCAs projection. 1.5  $\mu$ M PF8380 was injected locally into the thalamus of brain slices. The result showed that inhibition ATX in thalamic neuron did not alter the thalamocortical navigation in the CP (Figure 3.12D). The Chi-square test described that there was no significant difference between control and thalamus-inhibited slices (Figure 3.12E).

Moreover, the misrouted TCAs in PRG-2<sup>-/-</sup> animals did not result from any defect of the subplate neurons themselves. By the Ctgf (specific expression in subplate) antibody staining, the appearance of the subplate neurons in PRG-2<sup>-/-</sup> is normal (data in cooperation with Dr. A. Hoerder-Suabedissen). Taken together, these results suggest that the subplate-derived LPA, which is produced by ATX, contributes to correct guidance of thalamic fibers to the cortex.

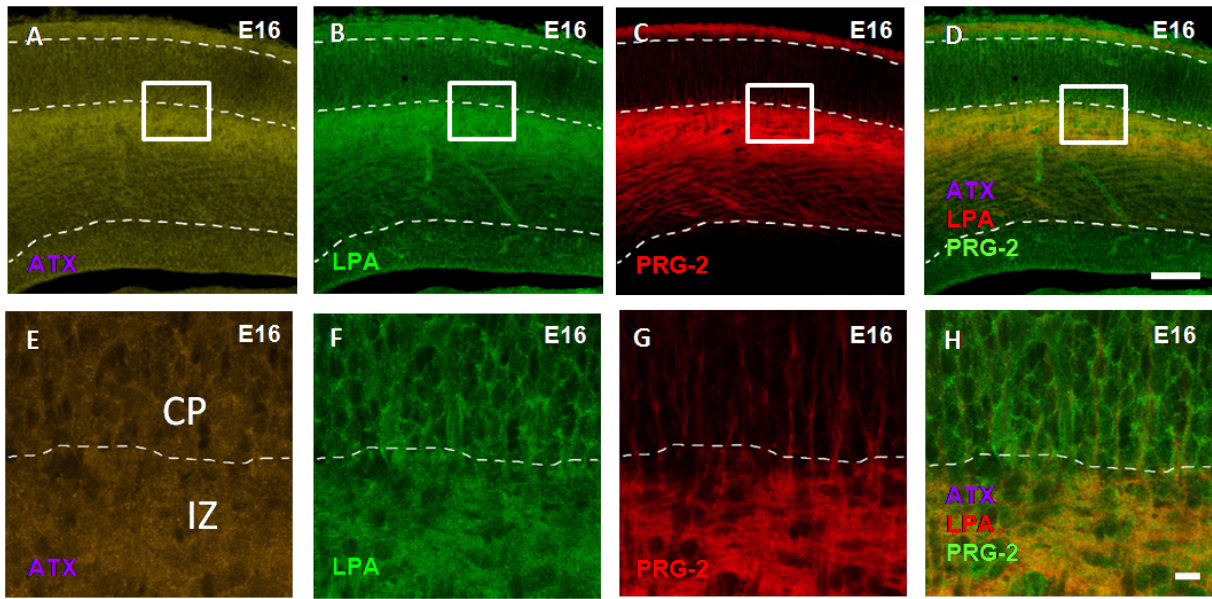


Figure 3.11 ATX and LPA express in the developing somatosensory cortex

(A-D) IHC results present strong ATX (A) and LPA (B) expression at the border of the E16 CP and the intermediate zone

(E-H) Higher-magnification image of the CP. Note that there are subplate neurons that coexpress ATX and LPA, but almost no PRG-2 expression in cortical neuron.

Scale bars represent 100 μm (A–D) and 10 μm (E–H)

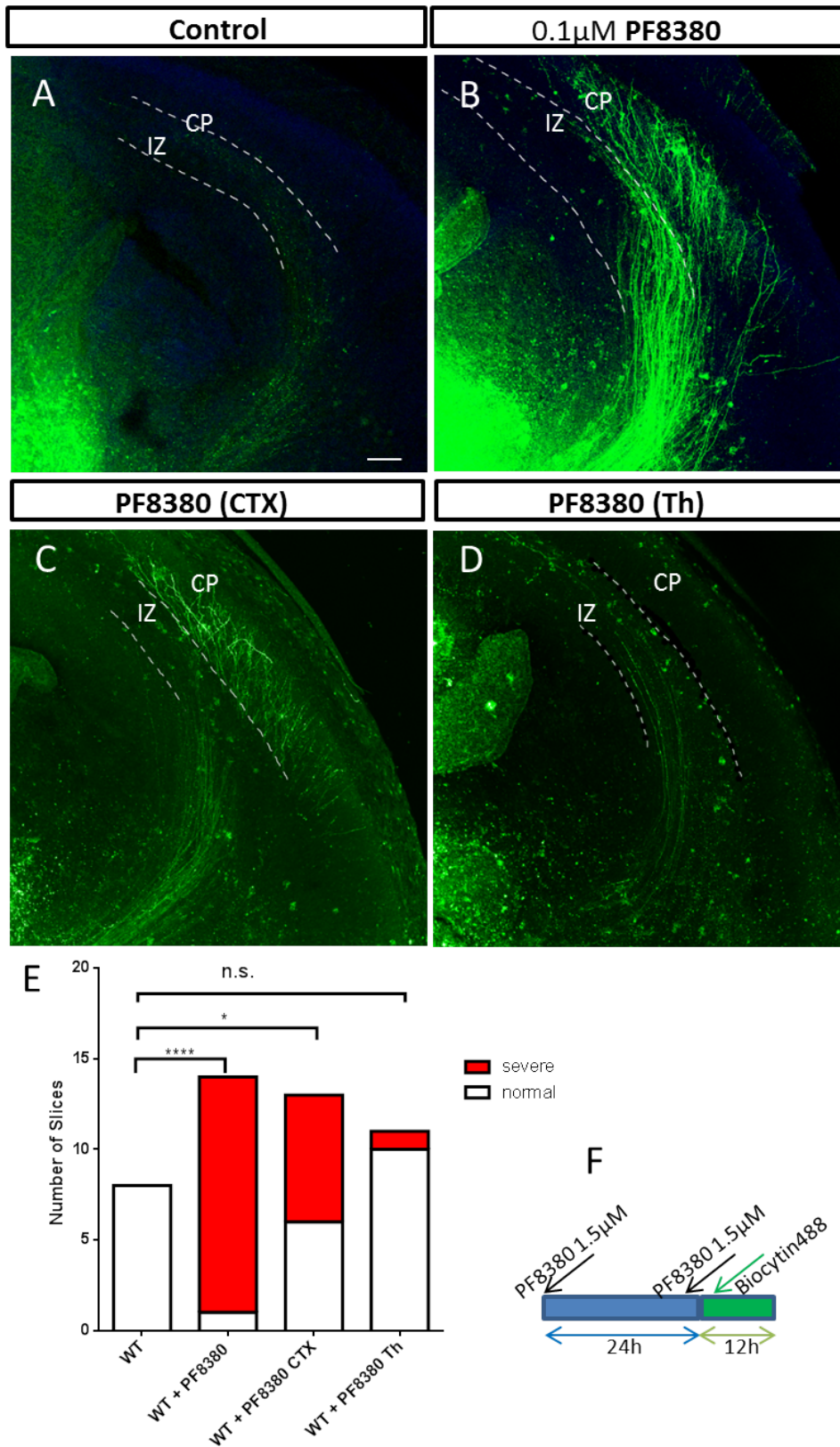


Figure 3.12 Inhibition of the LPA-synthesis enzyme Autotaxin (ATX) in cortex alters the TC projection in WT mice

(A and B) Biocytin-traced TCAs develop a normal fiber projection in WT slice (A). In contrast, slices from the same litter incubated with the ATX inhibitor PF8380 (applied to the medium) display a severe and aberrant TCAs (B).

(C) Cortical injection of PF8380 can lead to an aberrant thalamocortical fiber projection.

(D) Inhibition ATX in thalamus will not alter the WT thalamocortical fiber projection in CP.

(E) Analysis of aberrant termination of thalamocortical fibers under different conditions revealed significantly disturbed axon guidance after ATX inhibition (Fisher's exact test; number of slices = 8 WT, 14 WT + PF8380 applied to the culture media, 13 WT + cortical PF8380 injection, and 11 WT + thalamic PF8380 injection).

(F) Schematic drawing of the local injection of PF8380 in thalamocortical slices.

\* $p < 0.05$ , \*\*\*\* $p < 0.0001$ . Scale bars represent  $100\mu\text{m}$  (A–D)



### 3.6 PRG-2 mediates axonal sensitivity to LPA

To analyze the role of axonal PRG-2 in LPA-mediated thalamic axon guidance, E15 thalamic explants were embedded in 3D-matrigel with a polarized concentration of LPA and analyzed axonal outgrowth. 10  $\mu$ M fluorescent-labeled LPA (TF-LPA) mixed with matrigel was placed  $401.6 \pm 53.63 \mu\text{m}$  away from the WT explants border, or  $475 \pm 146.80 \mu\text{m}$  from the PRG-2<sup>-/-</sup>, while the adjacent side did not contain LPA (see Figure 3.13A and 3.13B for experimental design and Figure 3.13D<sub>2</sub> for the TF-LPA containing matrigel region at higher magnification).

In the 3D matrigel layer, thalamic explants started to grow neurites in 12 hrs culture, and thalamic axons extended radially after 24hr incubation. When thalamic axons were getting close to TF-LPA coating region, they would show characteristic alternations of growth and retraction. Subsequently, those growing fibers were analyzed according to the number of which innervate into the LPA-rich zone and the adjacent control zones. Higher magnification at the border towards the LPA-rich zone revealed that WT axons could not invade the LPA-rich zone (Figure 3.13C). On the other hand, PRG-2<sup>-/-</sup> axons grew far inside it (Figure 3.13D).

Quantitative analysis of fibers entering the LPA-rich zone into different distances (100  $\mu$ m and 200  $\mu$ m) revealed the significantly higher invasion from PRG-2<sup>-/-</sup> thalamic explants, while no difference between WT and PRG-2 axon fiber outgrowth was observed in the adjacent, non-LPA-containing control side (Figure 3.13E and 3.13F). Direct comparison of LPA-containing and control sides revealed that WT axons were significantly repelled by the LPA-rich zone. By contrast, PRG-2 deficiency caused axons to enter a LPA-rich zone, which could lead repulsive behavior to WT axons. These data suggested that PRG-2 was critically involved to mediate the sensitivity of thalamic axons to the repulsive guidance cue LPA.

During normal development, TCAs do not collapse at the border to the CP but rather maintain below the CP and continue to grow in the IZ until reaching their final target. This indicated that LPA provided by the subplate induced the turning of axon GCs when thalamocortical fibers approached LPA-rich areas. To mimic this situation in the outgrowth assay *in vitro*, thalamocortical explants also were exposed to lower LPA concentrations (1 $\mu$ M

LPA, Figure 3.13G). Compared to PRG-2<sup>-/-</sup> axons (Figure 3.13I), many WT axons displayed a typical turning behavior in front of the LPA-rich zone (Figure 3.13H).

To confirm this observation, live imaging of cultured TCAs was performed. Axon GCs were exposed to continuous and low concentration LPA (500nM LPA). To avoid bias caused by perfusion flow, which may repel axons, a LPA-containing matrigel-covered pipette tip was placed at distance of 40 μm from the GC tip. WT axons stopped growing and turned away from the LPA source (Figure 3.14A). In contrast, PRG-2<sup>-/-</sup> axons showed the normal growth, even attractive behavior to LPA (Figure 3.14B). Quantitative analysis revealed a distinct repulsion of WT axons to 500 nM LPA, which was not observed in PRG-2<sup>-/-</sup> axons (Figure 3.14C and 3.14D).

The same assay was performed to observe the GC response to Semaphorin 3A, a well-studied repulsive guidance cue. The result didn't suggest that PRG-2<sup>-/-</sup> axons lost the sensitivity to Semaphorin 3A (Figure 3.14E). Campbell and Holt (Campbell and Holt, 2001) studied the signaling pathway of Semaphorin 3A and LPA. It was discovered that both of chemotropic responses were induced by the cytoskeleton. The difference was that Semaphorin 3A-induced collapse could be blocked by inhibiting the protein synthesis. However, protein synthesis inhibitors did not block LPA-induced collapse. Their finding enhanced our understanding of LPA with a different signaling pathway to Semaphorin 3A. In summary, these data indicated that PRG-2 at the GC specifically mediated the repellent effect of LPA in axonal guidance.

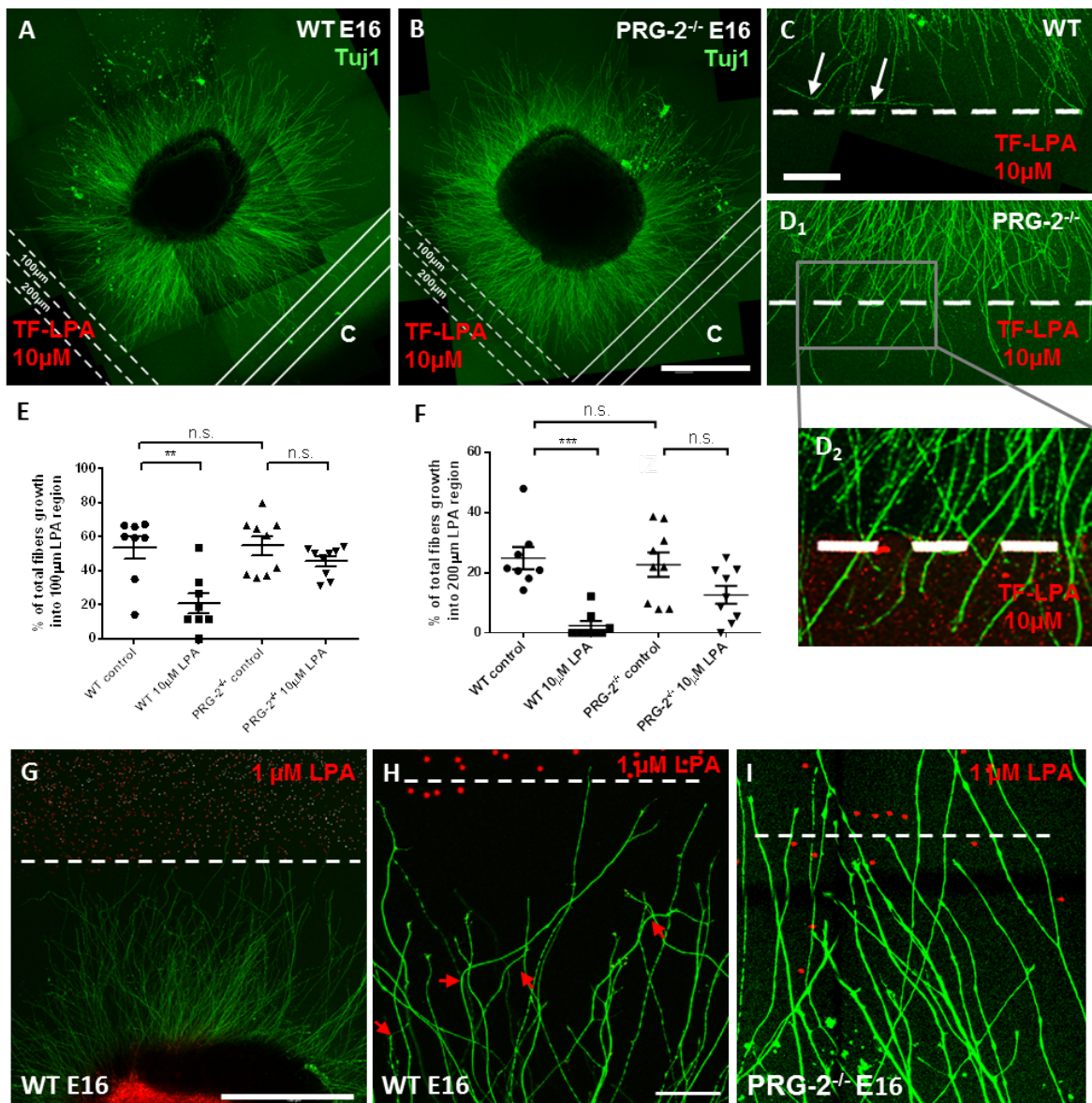


Figure 3.13 PRG-2 deficiency abolishes thalamic axon sensitivity to LPA

(A and B) Thalamic explants from WT (A) and PRG-2<sup>-/-</sup> (B) mice expose to 10 μM TF-LPA for 40 hrs. TF-LPA-containing zone is located in the lower left part of the explants. The LPA-free right side is regarded as control. Lines delineate regions locate 100 or 200 μm within the LPA-containing or the control region, respectively. Outgrowing axons stained for Tuj1 are color coded in green.

(C and D) Higher magnification of WT axons at the TF-LPA interface shows a repulsive effect on outgrowing axons (C, arrows). In contrast, PRG-2<sup>-/-</sup> axons are able to enter the LPA-

containing region (D1). Higher magnification shows the border of the TF-LPA-containing region color coded in red (D2).

(E-F) Quantitative analysis of percentage of fibers protruding into the 100  $\mu\text{m}$  (E) or 200  $\mu\text{m}$  (F) LPA-rich and control region (Kruskal-Wallis test with Dunn's multiple comparisons test; n = 8 WT and 9 PRG-2<sup>-/-</sup> thalamic explants)

(G and H) When exposed to lower LPA concentrations (1  $\mu\text{M}$ ; G), thalamic WT axons display a turning behavior (H; red arrows pointing to turning axons) in front of the LPA-rich region. Border of the LPA-rich zone is marked by dotted line and visible by addition of red fluorescent beads.

(I) Thalamic explants from PRG-2<sup>-/-</sup> mice at the border of the LPA-rich area display no turning behavior and entered the LPA-rich zone in high numbers.

\*p < 0.05, \*\*p < 0.01, \*\*\*p < 0.001. Bars represent mean  $\pm$  SEM.

Scale bars represent 500  $\mu\text{m}$  (A and B), 100 $\mu\text{m}$  (C and D1), 500 $\mu\text{m}$  (G) and 50 $\mu\text{m}$  (H and I)

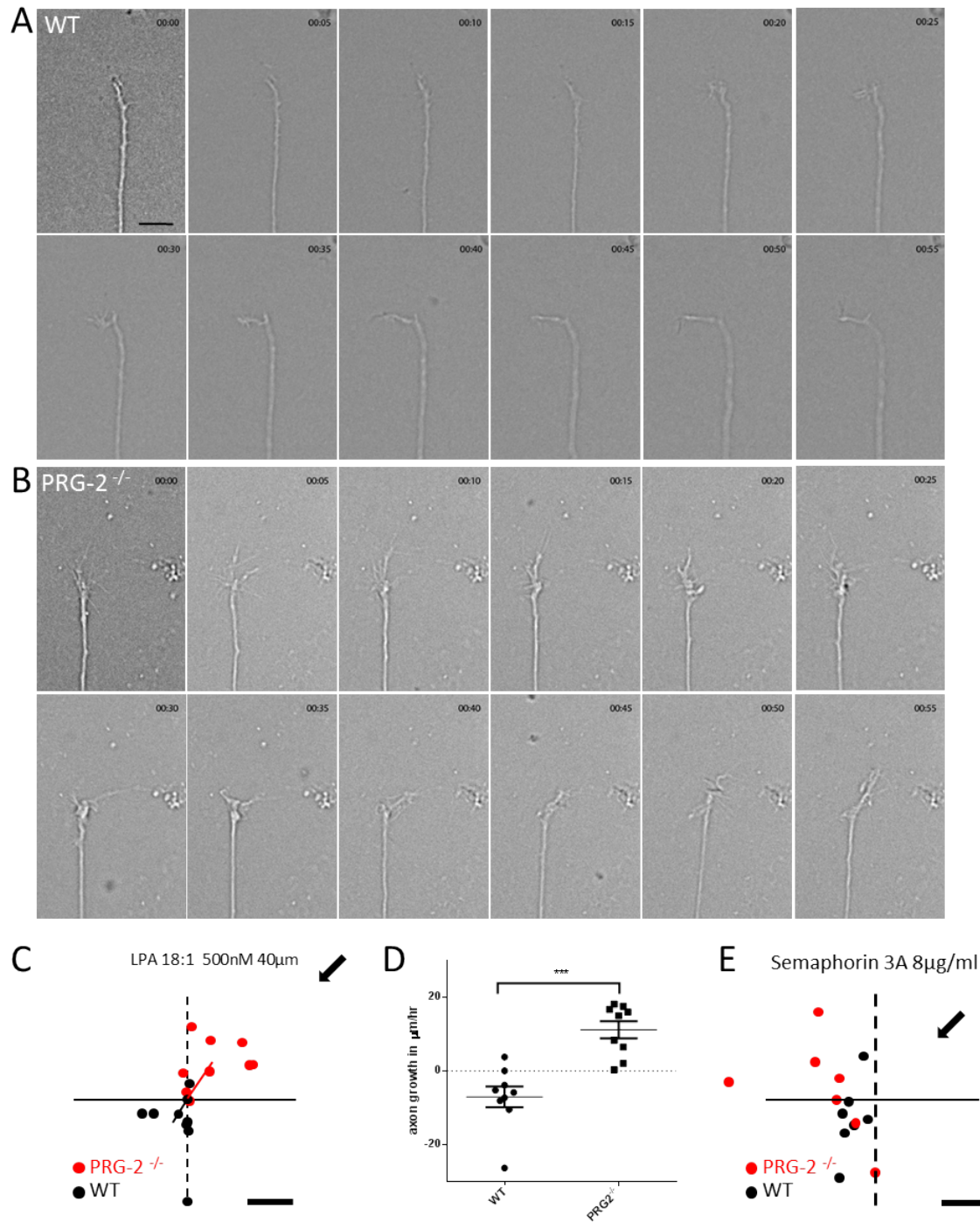


Figure 3.14 PRG-2 deficiency alters thalamic axon behavior to LPA

(A and B) Live imaging series of WT (A) and PRG-2<sup>-/-</sup> (B) GCs exposes to low LPA concentrations (500 nM) at a right-up distance of 40 μm for 60 mins

(C) Schematic diagram showing the starting and end points of GCs during live imaging. Axons extending during live imaging (60 min) into the quadrant facing the LPA source are assigned as positive values; axons growing in other quadrants are assigned as negative values.

(D) Analysis of GC behavior to LPA (Mann-Whitney test; n = 9 WT and 9 PRG-2<sup>-/-</sup> GCs).

(E) Schematic diagram showing starting point and end point of GCs faced to Semaphorin 3A during live imaging.

\*p < 0.05, \*\*p < 0.01, \*\*\*p < 0.001. Bars represent mean ± SEM.

Scale bars represent 10 μm (A, C and E).

### 3.7 Radixin (RDX) is a downstream PRG-2 interacting molecule in the axon GC

PRG-2 is a six-transmembrane molecule with an intracellular 400 amino acid-long C-terminal tail, which is believed to act in signal transduction. To determine putative interaction partners of this intracellular domain, our group had performed a Y2H screen using PRG-2 C-terminal tail as a bait and found a positive interaction with the FERM-domain of radixin (RDX) (Fehon et al., 2010). Using an anti-PRG-2 antibody for Immunoprecipitation (IP) on E17 brain lysate, it could be shown that PRG-2 interacted with RDX (Figure 3.15A). To further elucidate the role of this interaction in the guidance of thalamocortical fibers to the developing cortex, the proteins co-localization study was performed at E16 mouse brain. A high degree of co-expression of PRG-2 and RDX in the thalamocortical tract was detected in the IZ at E16 (Figure 3.15B and 3.15C). To prove that the RDX/PRG-2 interaction in fact occurred in the axon GC, the result by subcellular IF staining in cultured neurons showed that there was a strong signal of RDX and PRG-2 co-localization in GC (Figure 3.15D). Therefore, RDX was mainly expressed at the GC membrane and was co-localized with PRG-2.

RDX belongs to the Ezrin, Radixin and Moesin (ERM) protein family, containing a N-terminal band 4.1 protein and ERM (FERM) domain that directly bind to phosphatidylinositol 4,5-bisphosphate (PIP<sub>2</sub>) at the plasma membrane. The C-terminal of RDX can directly bind to filamentous actin (F-actin), thereby acting as a crosslinker between the cortical F-actin-cytoskeleton and the plasma membrane (Fehon et al., 2010). The C-terminal and FERM domain of RDX need to be in its open and active conformation, which is elicited *in vivo* by phosphorylation of threonine residue at position 564 (T564). This characteristic phosphorylation in the C-terminal which leads protein to unfold is highly conserved in the ERM protein family (Pearson et al., 2000). Their activated form is called pERM. Meanwhile, its active status allows RDX to bind to the cytoplasmic tail of transmembrane protein. Therefore, the role of PRG-2 in RDX activation could be studied using a specific antibody which recognized the phosphorylation of T564 in RDX, T567 in Ezrin and T558 in Moesin (Hausrat et al., 2015).

Compared to WT neurons, pERM levels in PRG-2<sup>-/-</sup> neurons was significantly lower (Figure 3.15E and 3.15F), indicating a diminished activation of ERM proteins. To prove the role of

LPA in ERM activation, pERM levels over time was analyzed. ERM phosphorylation was increased fast and constantly over time under LPA stimulation (Figure 15G and 15H). The effect of different LPA concentrations was further assessed. Starting with 100 nM, which already revealed an increase in ERM phosphorylation, 1  $\mu$ M LPA induced a significant and robust increase in pERM levels (Figure 3.15I and 3.15J).

To answer the question of whether RDX/PRG-2 association at the membrane was important for LPA-dependent RDX phosphorylation in neurons, the effect of LPA stimulation on pERM expression in WT and PRG-2<sup>-/-</sup> neurons was compared. As a result, LPA stimulation of WT neurons could give rise to a significant increase in pERM levels, while PRG-2<sup>-/-</sup> neurons failed to show any significant change (Figure 3.15K and 3.15L). These results point to a yet unknown, but critical role of PRG-2 in mediating LPA-induced RDX activation.



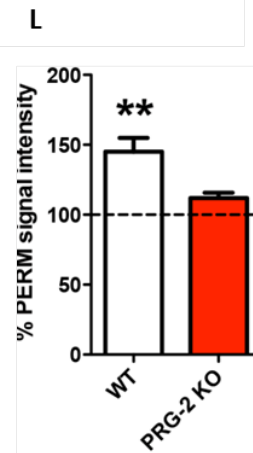
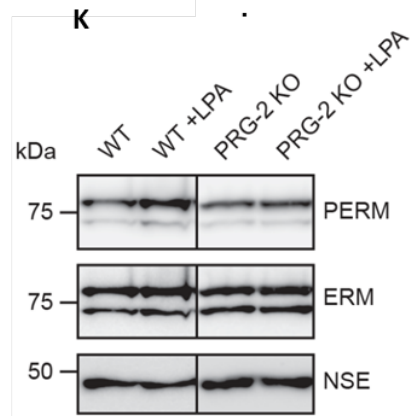
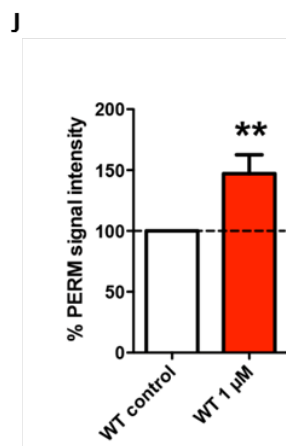
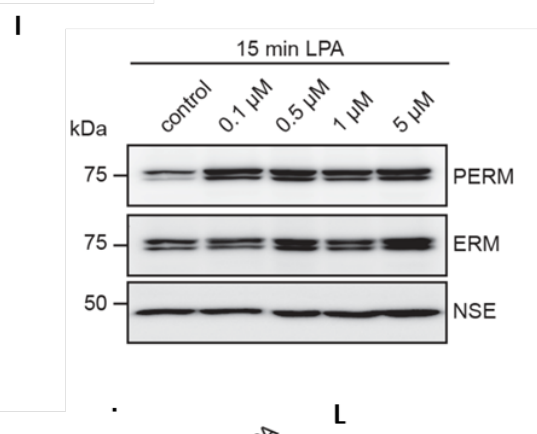
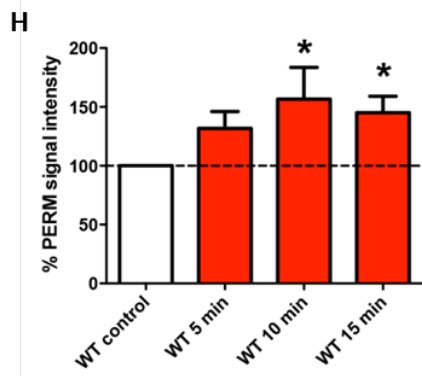
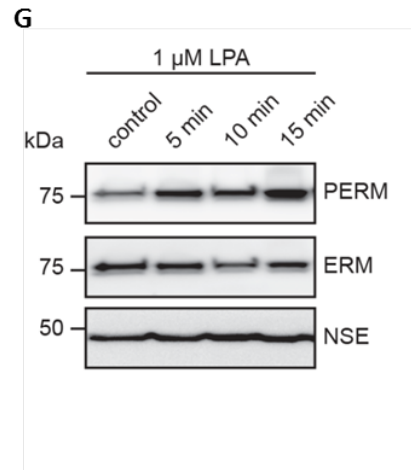
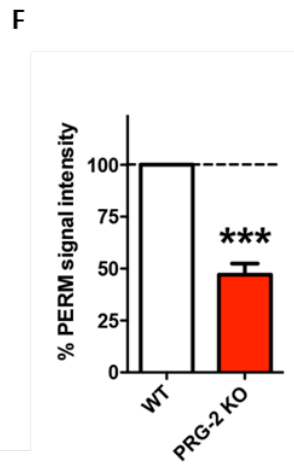
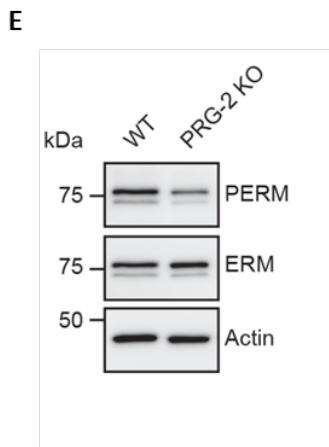
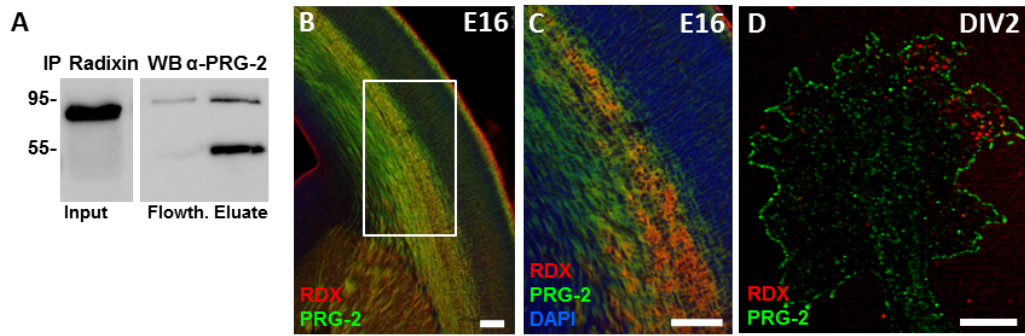


Figure 3.15 PRG-2 Interacts with RDX and mediates LPA-dependent ERM activation in cortical Neurons

(A) CoIP of RDX and PRG-2 from E17 brain lysates. Antibodies against RDX co-precipitate PRG-2. Signal below PRG-2 band represents heavy chains of the antibody used for IP.

(B) RDX and PRG-2 show clear co-localization along the thalamocortical tract at E16.

(C) Higher magnification of (B).

(D) PRG-2 and RDX are mainly localized at the GC tips.

(E and F) Western blot of PRG-2<sup>-/-</sup> neurons cultivated for 7 days (DIV7; E) shows a lower expression of phosphorylated ERM (pERM) when compared to WT controls (F; one-sample t test; n = 5 cultures per genotype).

(G and H) Western blot of DIV7 WT neurons stimulated with 1 μM LPA (G) shows significantly increased pERM levels starting 10 min after LPA stimulation (H; one-way ANOVA with Bonferroni correction; n = 18 cultures for 0 and 15 min, n = 9 cultures for 5 and 10 min).

(I and J) Western blot (I) and quantification of pERM levels in DIV7 WT neurons stimulated for 15 min with 1 μM LPA (J; one-sample t test; n = 9 cultures per group).

(K and L) Western blot (K) of PRG-2<sup>-/-</sup> neurons stimulated with LPA (1 μM for 15 min) does not display altered pERM levels (L; one-sample t test; n = 18 WT and n=7 PRG-2<sup>-/-</sup>).

\*p < 0.05, \*\*p < 0.01, \*\*\*p < 0.001. Bars represent mean ± SEM.

Scale bars represent 100 (B and C) and 1 μm (D).

### 3.8 PRG-2 mediates pERM increase at GC membranes induced by extracellular LPA

RDX is concentrated below the plasma membrane, a critical position linking transmembrane signaling to the actin cytoskeleton. Since phosphorylation influences RDX activity in connecting the actin-cytoskeleton with the membrane (Matsui et al., 1998), transmembrane signaling events leading to RDX activation are optimally suited to act in extracellular cue mediated axon guidance. Therefore, the effect of extracellular LPA on pERM changes at the GC in WT and PRG-2<sup>-/-</sup> neurons was analyzed. As shown in Figure 3.16B and 3.16F, pERM in WT GCs was concentrated in a compartment directly adjacent to the GC leading membrane and strongly increased upon LPA stimulation. In contrast, no change of pERM was observed in PRG-2<sup>-/-</sup> GCs (Figure 3.16D and 3.16H). Quantitative analysis of pERM levels confirmed these observations (Figure 3.16I). Moreover, direct comparison of pERM levels in the center of the GC and in the periphery revealed a compartmentalization of the pERM signal at the membrane of WT GCs but not of PRG-2<sup>-/-</sup> GCs (Figure 3.16J). This enriched localization of pERM at the GC tip supports the concept of a critical role of pERM in GC behavior.

To prove that ERM phosphorylation and activation play a role in LPA-induced GC turning, the subcellular localization of pERM in GCs of thalamic explants exposed to an LPA-rich environment (1 $\mu$ M LPA) was analyzed by live imaging. RDX fused with GFP was firstly transfected into WT and PRG-2<sup>-/-</sup> hippocampal neurons in DIV1. Then in DIV3 GCs were observed by confocal microscopy. In the WT GC, the RDX accumulated in the center with no treatment (Figure 3.17A). When locally placing LPA for 20 mins by the coated glass pipette at a distance of 40  $\mu$ m, RDX dynamically moved close to the GC membrane (Figure 3.17B). In comparison, RDX in PRG-2<sup>-/-</sup> GC did not show any active translocation during extracellular LPA-stimulation (Figure 3.17C and 3.17D).

Meanwhile, RDX<sup>GFP</sup> and F-actin tagged RFP were transfected in WT hippocampal neurons. Detailed analysis of turning GCs encircled in Figure 3.18A revealed strong RDX signal co-localized with F-actin at the tip of the GC. When RDX was delivered to the GC membrane, the F-actin also accumulated in this point and started to grow into a new filopodium tip. Finally, the growing GC turned away from the LPA-rich zone (Figure 3.18A-3.18C). Mintz *et al.* discovered that total ERM proteins are distributed more symmetrically in the periphery of

cortical growth cone than phosphorylated ERM. The strong asymmetry pERM influenced axon turning in response to localized guidance cue (Mintz et al., 2008). Taken together, these results confirmed the critical role of PRG-2/RDX interaction for RDX activation which eventually led to axon turning with the stimulation of extracellular LPA.

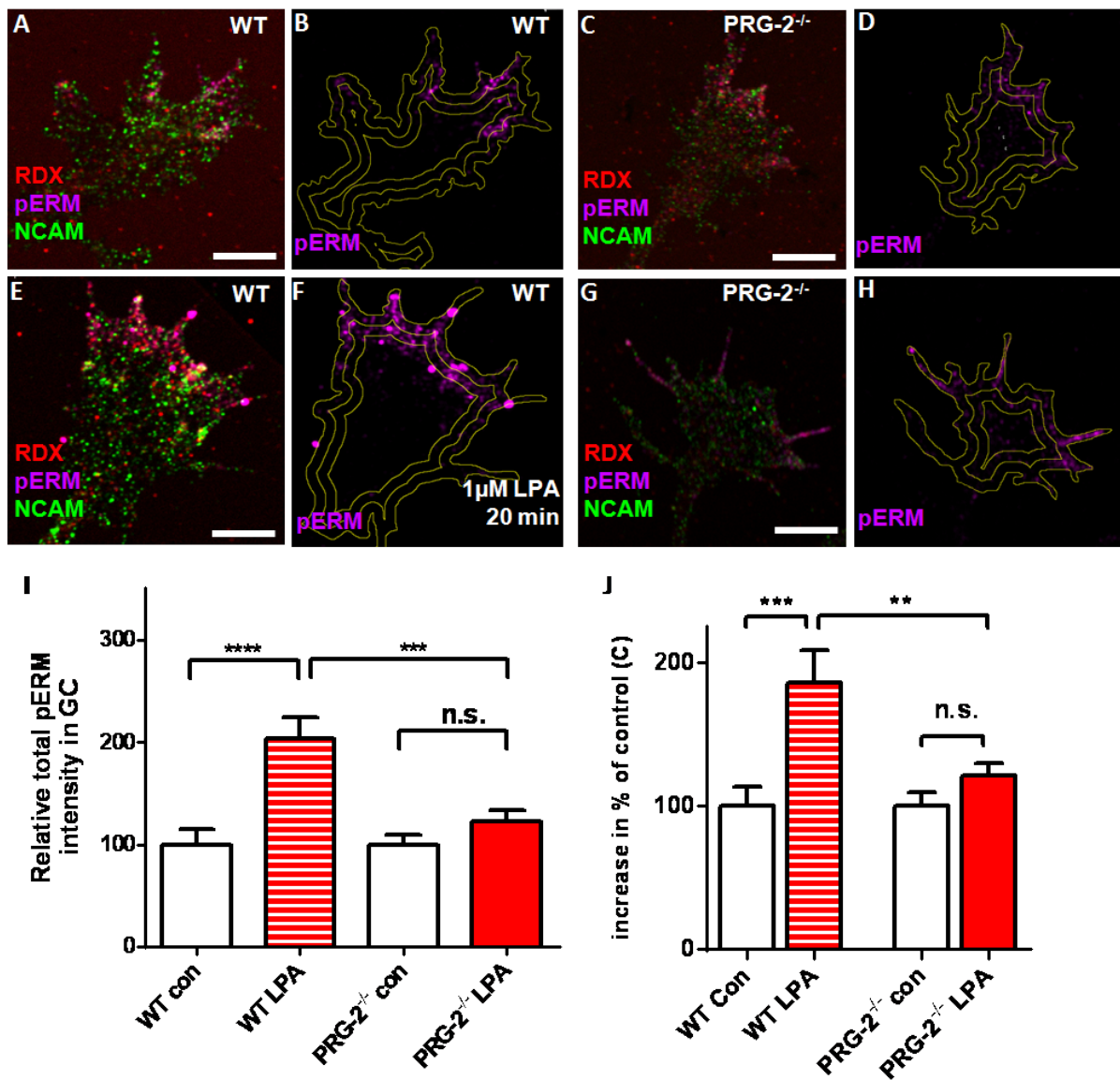


Figure 3.16 PRG-2 induces LPA-dependent pERM expression at the GC Membrane

(A–H) RDX, pERM, and NCAM expression in WT GC without (A and B) and with (E and F) 1  $\mu$ M LPA stimulation in the DIV2 neuronal culture. Note the prominent pERM expression located at the WT GC membrane (F). LPA stimulation didn't increased pERM expression at the PRG-2<sup>-/-</sup> GC membrane (C, D, G and H).

(I) Signal intensity analyses of pERM at the GC membrane upon LPA stimulation (Kruskal-Wallis test with Dunn's multiple comparisons test; number of analyzed GCs = 21 non-stimulated and 23 stimulated WT GCs, and 22 non-stimulated and 24 stimulated PRG-2<sup>-/-</sup> GCs).

(J) Ratio of pERM expressed in the GC center and in the periphery significantly increased upon LPA stimulation in WT GCs, while no change was observed in PRG-2<sup>-/-</sup>GCs (one-way ANOVA with Bonferroni correction; number of analyzed GCs = 21 non-stimulated and 20 stimulated WT GCs, and 22 non-stimulated and 24 stimulated PRG-2<sup>-/-</sup> GCs).

\*\*p < 0.01, \*\*\*p < 0.0001. Bars represent mean ± SEM. Scale bars, 5 μm.

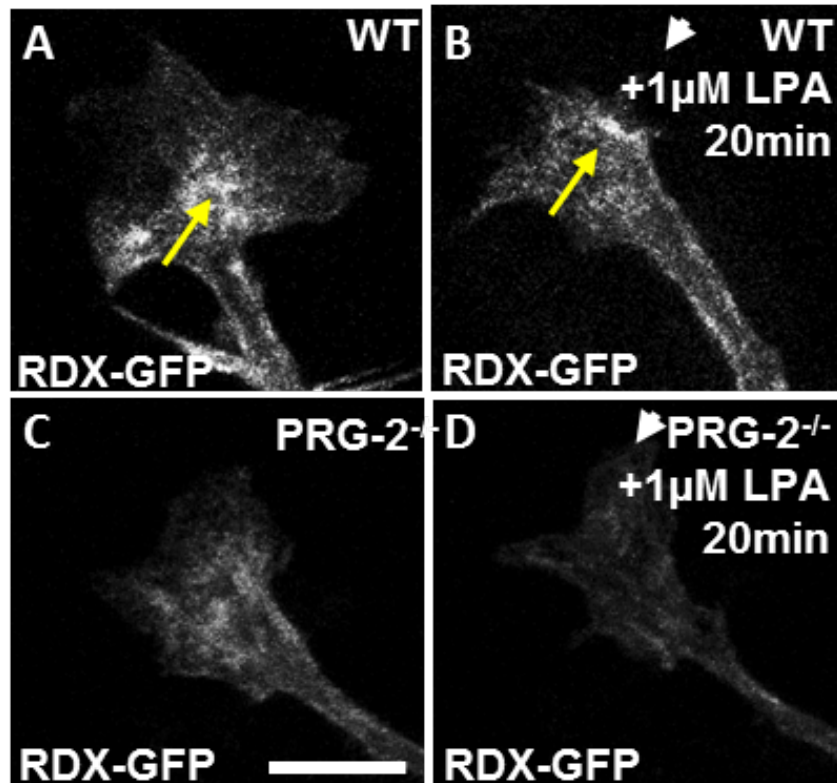


Figure 3.17 Live imaging of RDX-GFP GC in the LPA stimulation

(A and B) RDX-GFP-transfected GC of a WT neuron at DIV2 before (A) and 20 min after 1  $\mu$ M LPA stimulation (B). White arrow indicates site of LPA stimulation (LPA at a distance of 40  $\mu$ m); yellow arrow indicates RDX-GFP translocation from the GC center to the GC periphery at the site of the LPA application.

(C and D) RDX-GFP distribution in a PRG-2<sup>-/-</sup> neuron at DIV2 before (C) and after LPA stimulation (D) is not markedly changed.

Scale bar represents 5  $\mu$ m (A-D)

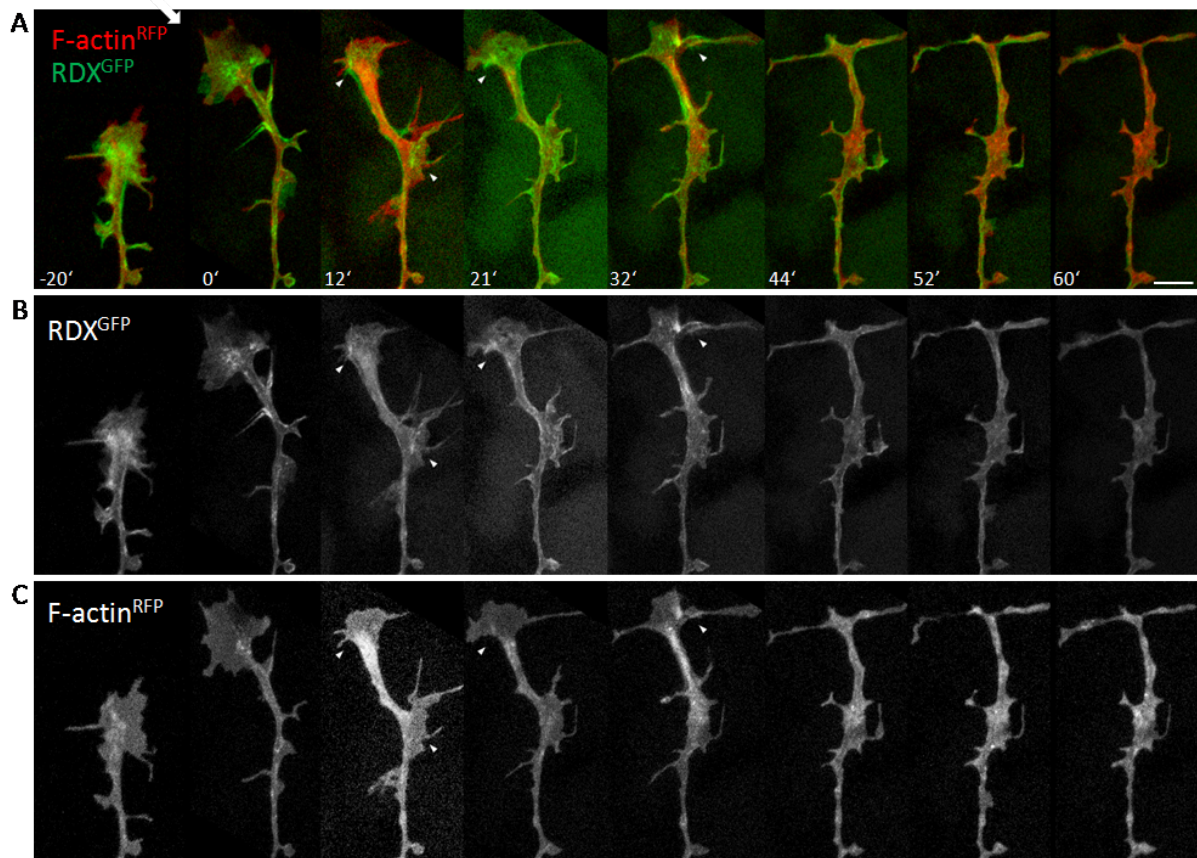


Figure 3.18 Time-lapse fluorescence microscopy of double-labeled neural GC during LPA stimulation

(A) GC expressing RDX-GFP (B; green) and F-actin-RFP (C; red). White arrow indicates site of LPA stimulation. When stimulated by LPA, RDX accumulates at the GC membrane (White arrowheads).

Scale bar represents 5  $\mu\text{m}$  (A-D)



### 3.9 RDX-deficiency phenocopies PRG-2 thalamocortical axon defect

To further substantiate the role of RDX in LPA-induced GC turning, the thalamocortical projection in RDX<sup>-/-</sup> mice was analyzed. Using biocytin tracing in living E17 thalamocortical slices, misrouted thalamocortical projection in RDX<sup>-/-</sup> slices was observed, which aberrantly invaded the CP (Figure 3.19B and 3.19B') in the same way as PRG-2<sup>-/-</sup> mice, while in the control littermates thalamocortical projection normally confined to the IZ (Figure 3.19A). Quantitative analysis confirmed the severe phenotype of aberrant projection in RDX-deficient thalamocortical slices (Figure 3.19E).

Meanwhile, the PRG-2<sup>+/-</sup>/RDX<sup>+/-</sup> mice were traced in the same way. Those transheterozygous slices also showed deficient thalamocortical projections due to the decreased PRG-2/RDX interaction (Figure 3.19D, 3.19D' and 3.19F). These data enhanced the idea that the LPA-PRG-2-RDX/pERM signal transduction axis is critical to correct guidance and restriction of TCAs to the IZ, thereby avoiding their premature and aberrant entry into inappropriate cortical compartments (Figure 3.20).

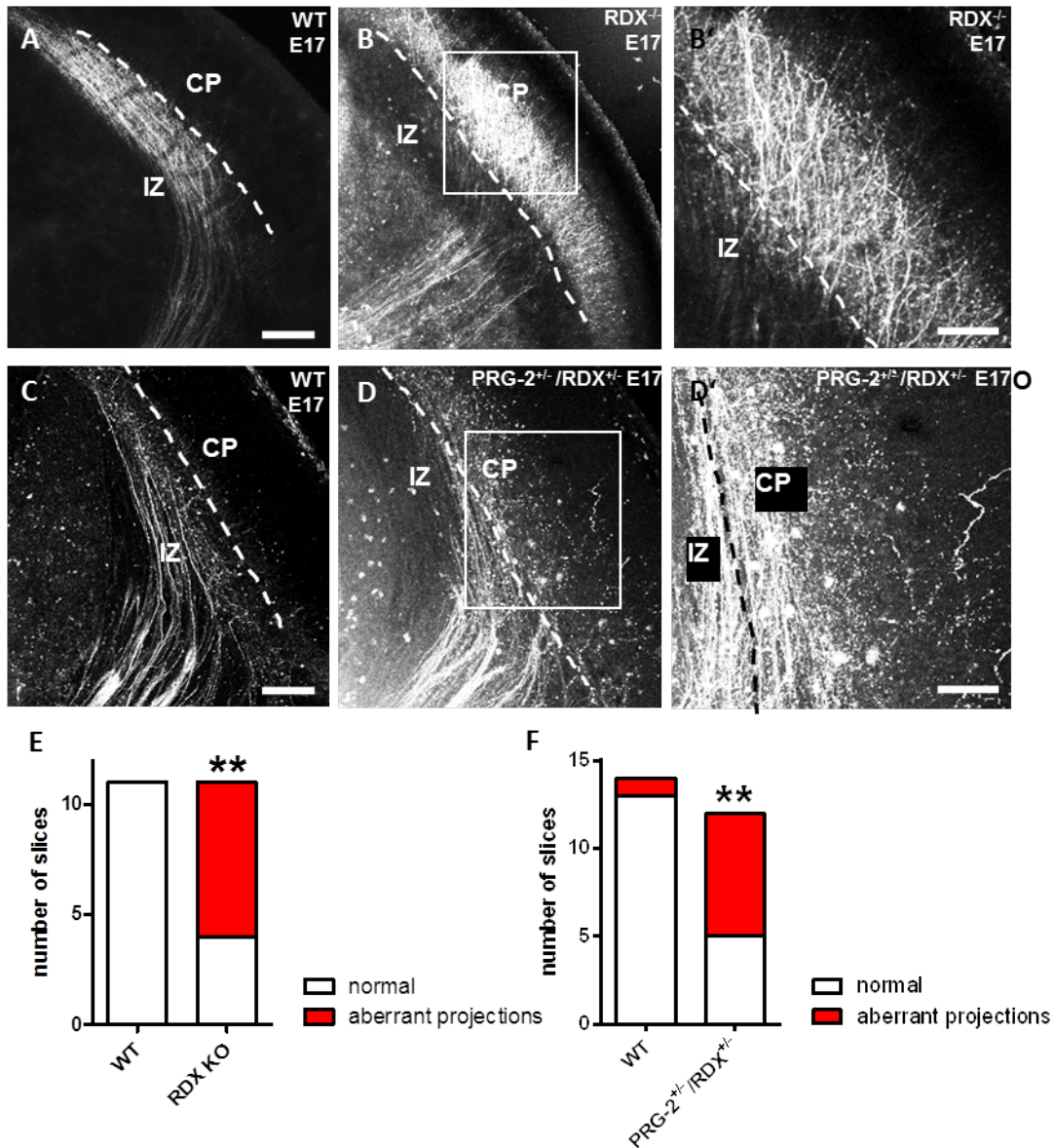


Figure 3.19 RDX<sup>-/-</sup> and PRG-2<sup>+/-</sup>/RDX<sup>+/-</sup> slices phenocopy PRG-2<sup>-/-</sup> thalamocortical defect (A-B') Biocytin tracing reveals normal distributed thalamocortical fibers in WT slices (A) but an aberrant projection in RDX<sup>-/-</sup> slices (B). Higher magnification of aberrant fibers is shown in (B'). Quantitative analysis is shown in (E) (Fisher's exact test; n = 11 WT and 11 RDX<sup>-/-</sup> slices). (C-D') Biocytin tracing in thalamocortical slices from WT (C) and PRG-2<sup>+/-</sup>/RDX<sup>+/-</sup> animals (D and D') at E17 shows an altered thalamocortical projection in PRG-2<sup>+/-</sup>/RDX<sup>+/-</sup> slices. Quantitative analysis is shown in (F). (Fisher's exact test; n = 14 WT and 12 PRG-2<sup>+/-</sup>/RDX<sup>+/-</sup> slices).

\*\*p < 0.01. Scale bars represent 200  $\mu$ m (A-D) and 100  $\mu$ m (B' and D').

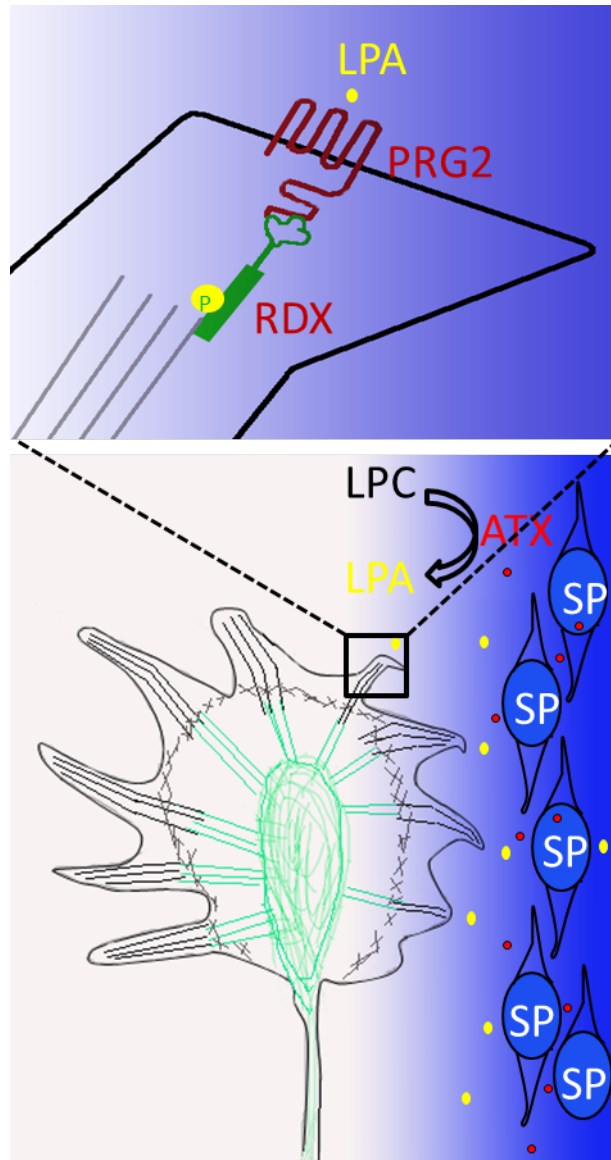


Figure 3.20 Schematic representation of LPA-PRG-2-RDX/pERM signaling pathway

## 4 Discussion

In the mammalian forebrain, thalamus relays sensory and motor information to the cerebral cortex as the exchange center and transduces the modulatory input back from cortex (López-Bendito and Molnár 2003). Individual thalamic nucleus specifically delivers peripheral sensory input to certain area of the cortex. Well-organized thalamocortical projections develop from the embryonic stage to the early postnatal time. When TCAs arrive at the telencephalon of E14 mice brains, they accumulate in the IZ and subplate, below the CP (Ghosh et al., 1990; Molnar et al., 1998). Here, they interact with a transient neuronal population, the subplate neurons, which keep them in place and are thereby critically important for correct patterning of the thalamocortical connections (Ghosh and Shatz, 1993). Thalamic axons invade and innervate layer IV of inappropriate cortical regions as a result of subplate ablation in the immature cortex (Ghosh and Shatz, 1993; McConnell et al., 1994; Tolner et al., 2012). Although the role of subplate neurons has long been recognized (Kanold and Luhmann, 2010) and gene expression patterns of subplate neurons have been described (for review see (Hoerder-Suabedissen and Molnar, 2015)), the molecular mechanisms regulating the subplate neurons/thalamocortical fiber interaction are far from being understood.

In this study, the role of PRG-2 in the developing TCAs was analyzed. The results showed that the TCAs in embryonic ages extended beyond the IZ and the subplate, and prematurely and aberrantly entered the CP. The underlying molecular mechanism was explored. The results showed that PRG-2 KO TCAs lost the sensitivity to LPA, which was produced by the subplate-secreted ATX. Further signaling pathway studies verified that ATX/LPA/PRG-2/pRDX signaling pathway affected the distribution of F-actin cytoskeleton in GCs of TCAs.

### **Role of phospholipids in subplate/thalamocortical axon interaction**

Subplate neurons play an important role in the functional and structural development of TCAs (Tolner et al., 2012). Due to the missing guidance by the subplate at embryonic ages, PRG-2-deficient TCAs in both PRG-2 null and thalamus-specific KO mouse brains formed an

aberrant projection, which prematurely innervated CP. This misrouted projection directly altered the correct targeting and integration of TCAs into layer IV as shown by fibers tracing at young postnatal ages. PRG-2 is necessary to the development of TCAs, which navigates and maintains TCAs in the IZ at the early embryonic stage as a LPA sensor. Subplate contains some of the earliest generated neurons and is the dynamic transient zone in the neocortex. By the microarrays analysis, many genes which high-fold enriched in subplate were identified (Hoerder-Suabedissen et al., 2013). One of those genes is *ATX*, which is specifically expresses in the subplate neurons as the major producer of LPA. When *ATX* activity of the cortex was blocked by locally injecting PF8380 in the WT brain culture slices, the same phenotype as described in the PRG-2-deficient was observed in the study. The critical importance of PRG-2-mediated extracellular LPA effects on thalamic axon guidance was further clarified by single axon analyses. According to the results of axon growth assays, the fibers of WT thalamic neurons presented repelled behaviors to LPA as described in the previous work (Campbell and Holt, 2001; Yuan et al., 2003), while PRG-2<sup>-/-</sup> fibers lost the repulsive sensitivity to LPA. However, PRG-2<sup>-/-</sup> fibers still can be evoked repulsive response to *Sema3A* as the same as WT. In line with live imaging data, the axon of WT thalamic explants *in vitro* were repelled/collapsed when in contact with LPA, while lower LPA concentrations (1μM) induced a turning behavior in GCs. However, PRG-2<sup>-/-</sup> axons were not affected even by high LPA concentrations (10μM). Those data suggest a thalamocortical guidance mechanism with a mutual dependence on LPA/PRG-2 interaction.

### **RDX, an F-actin interacting molecule, is the downstream executor of LPA/PRG-2-dependent axon guidance**

While downstream mechanisms mediating LPA GC collapse have been described (Campbell and Holt, 2003; Zhang et al., 2003), direct and specific LPA interacting molecules involved in this mechanism remain unclear. Searching for downstream interacting partners, RDX was identified with direct interaction and co-expression with PRG-2 in TCAs. In cultured WT neurons, low concentration LPA as 100 nM could induce clear RDX phosphorylation. However, RDX phosphorylation in PRG-2<sup>-/-</sup> neurons did not increase, even upon 15min of 1μM LPA stimulation. The significant difference suggested PRG-2 was critically important for

RDX activation by extracellular LPA. Moreover, LPA-stimulation induced strong ERM phosphorylation at the GC membrane of WT axons, while PRG-2 deficient GCs failed to show these changes. The signaling axis LPA/PRG-2/RDX is responsible for axon turning since pERM adjacent to F-actin is detected at the tip of the turning GC. Live imaging showed that the labeled RDX in WT GC localized to the membrane and changed the cytoskeleton distribution when treating LPA locally. However, PRG-2-deficient GC did not show a dynamic RDX translocation. Together these results provide important insights into a clear LPA/PRG-2/RDX signal transduction axis, which is the critical pathway for axon guidance.

LPA in the dorsal telencephalon is considered as an extracellular guidance molecule interacted with PRG-2, which plays an important role in signaling transduction and navigate TCAs in IZ at the early embryonic developmental stage. When the GC is stimulated by LPA, it presents a repulsive response as a result of PRG-2 activating downstream RDX and inducing the redistribution of cytoskeleton.

## References

- Andrews, W., Liapi, A., Plachez, C., Camurri, L., Zhang, J., Mori, S., Murakami, F., Parnavelas, J.G., Sundaresan, V., and Richards, L.J. (2006). Robo1 regulates the development of major axon tracts and interneuron migration in the forebrain. *Development* 133, 2243-2252.
- Antoine-Bertrand, J., Ghogha, A., Luangrath, V., Bedford, F.K., and Lamarche-Vane, N. (2011). The activation of ezrin-radixin-moesin proteins is regulated by netrin-1 through Src kinase and RhoA/Rho kinase activities and mediates netrin-1-induced axon outgrowth. *Molecular biology of the cell* 22, 3734-3746.
- Birgbauer, E., and Chun, J. (2010). Lysophospholipid receptors LPA are not required for the inhibitory effects of LPA on mouse retinal growth cones. *Eye and brain* 2, 1-13.
- Blockus, H., and Chedotal, A. (2014). The multifaceted roles of Slits and Robos in cortical circuits: from proliferation to axon guidance and neurological diseases. *Current opinion in neurobiology* 27, 82-88.
- Bonnin, A., Torii, M., Wang, L., Rakic, P., and Levitt, P. (2007). Serotonin modulates the response of embryonic thalamocortical axons to netrin-1. *Nature neuroscience* 10, 588-597.
- Braisted, J.E., Catalano, S.M., Stimac, R., Kennedy, T.E., Tessier-Lavigne, M., Shatz, C.J., and O'Leary, D.D.M. (2000). Netrin-1 promotes thalamic axon growth and is required for proper development of the thalamocortical projection. *Journal of Neuroscience* 20, 5792-5801.
- Brauer, A.U., and Nitsch, R. (2008). Plasticity-related genes (PRGs/LRPs): a brain-specific class of lysophospholipid-modifying proteins. *Biochimica et biophysica acta* 1781, 595-600.
- Brauer, A.U., Savaskan, N.E., Kuhn, H., Prehn, S., Ninnemann, O., and Nitsch, R. (2003). A new phospholipid phosphatase, PRG-1, is involved in axon growth and regenerative sprouting. *Nature neuroscience* 6, 572-578.
- Bretscher, A., Edwards, K., and Fehon, R.G. (2002). ERM proteins and merlin: Integrators at the cell cortex. *Nat Rev Mol Cell Bio* 3, 586-599.
- Brindley, D.N., and Pilquil, C. (2009). Lipid phosphate phosphatases and signaling. *Journal of lipid research* 50 Suppl, S225-230.
- Brown, A., Brown, S., Ellisor, D., Hagan, N., Normand, E., and Zervas, M. (2009). A practical approach to genetic inducible fate mapping: a visual guide to mark and track cells in vivo. *Journal of visualized experiments : JoVE*.
- Campbell, D.S., and Holt, C.E. (2001). Chemotropic responses of retinal growth cones mediated by rapid local protein synthesis and degradation. *Neuron* 32, 1013-1026.

Campbell, D.S., and Holt, C.E. (2003). Apoptotic pathway and MAPKs differentially regulate chemotropic responses of retinal growth cones. *Neuron* 37, 939-952.

Cirulli, V., and Yebra, M. (2007). Netrins: beyond the brain. *Nature reviews Molecular cell biology* 8, 296-306.

Contos, J.J., Fukushima, N., Weiner, J.A., Kaushal, D., and Chun, J. (2000). Requirement for the IpA1 lysophosphatidic acid receptor gene in normal suckling behavior. *Proceedings of the National Academy of Sciences of the United States of America* 97, 13384-13389.

Deck, M., Lokmane, L., Chauvet, S., Mailhes, C., Keita, M., Niquille, M., Yoshida, M., Yoshida, Y., Lebrand, C., Mann, F., *et al.* (2013). Pathfinding of Corticothalamic Axons Relies on a Rendezvous with Thalamic Projections. *Neuron* 77, 472-484.

Deming, P.B., Campbell, S.L., Stone, J.B., Rivard, R.L., Mercier, A.L., and Howe, A.K. (2015). Anchoring of Protein Kinase A by ERM (Ezrin-Radixin-Moesin) Proteins Is Required for Proper Netrin Signaling through DCC (Deleted in Colorectal Cancer). *J Biol Chem* 290, 5783-5796.

Demyanenko, G.P., Siesser, P.F., Wright, A.G., Brennaman, L.H., Bartsch, U., Schachner, M., and Maness, P.F. (2011). L1 and CHL1 Cooperate in Thalamocortical Axon Targeting. *Cerebral cortex* 21, 401-412.

Erzurumlu, R.S., Chen, Z.F., and Jacquin, M.F. (2006). Molecular determinants of the face map development in the trigeminal brainstem. *The anatomical record Part A, Discoveries in molecular, cellular, and evolutionary biology* 288, 121-134.

Erzurumlu, R.S., and Gaspar, P. (2012). Development and critical period plasticity of the barrel cortex. *The European journal of neuroscience* 35, 1540-1553.

Estivill-Torres, G., Llebreg-Zayas, P., Matas-Rico, E., Santin, L., Pedraza, C., De Diego, I., Del Arco, I., Fernandez-Llebreg, P., Chun, J., and De Fonseca, F.R. (2008). Absence of LPA1 signaling results in defective cortical development. *Cerebral cortex* 18, 938-950.

Fehon, R.G., McClatchey, A.I., and Bretscher, A. (2010). Organizing the cell cortex: the role of ERM proteins. *Nature reviews Molecular cell biology* 11, 276-287.

Fincher, J., Whiteneck, C., and Birgbauer, E. (2014). G-protein-coupled receptor cell signaling pathways mediating embryonic chick retinal growth cone collapse induced by lysophosphatidic acid and sphingosine-1-phosphate. *Developmental neuroscience* 36, 443-453.

Ghosh, A., Antonini, A., McConnell, S.K., and Shatz, C.J. (1990). Requirement for subplate neurons in the formation of thalamocortical connections. *Nature* 347, 179-181.

Ghosh, A., and Shatz, C.J. (1993). A role for subplate neurons in the patterning of connections from thalamus to neocortex. *Development* 117, 1031-1047.



Gierse, J., Thorarensen, A., Beltey, K., Bradshaw-Pierce, E., Cortes-Burgos, L., Hall, T., Johnston, A., Murphy, M., Nemirovskiy, O., Ogawa, S., *et al.* (2010). A novel autotaxin inhibitor reduces lysophosphatidic acid levels in plasma and the site of inflammation. *The Journal of pharmacology and experimental therapeutics* *334*, 310-317.

Greenman, R., Gorelik, A., Sapir, T., Baumgart, J., Zamor, V., Segal-Salto, M., Levin-Zaidman, S., Aidinis, V., Aoki, J., Nitsch, R., *et al.* (2015). Non-cell autonomous and non-catalytic activities of ATX in the developing brain. *Frontiers in neuroscience* *9*, 53.

Guan, C.B., Xu, H.T., Jin, M., Yuan, X.B., and Poo, M.M. (2007). Long-range Ca<sup>2+</sup> signaling from growth cone to soma mediates reversal of neuronal migration induced by slit-2. *Cell* *129*, 385-395.

Hall, A., and Lalli, G. (2010). Rho and Ras GTPases in axon growth, guidance, and branching. *Cold Spring Harbor perspectives in biology* *2*, a001818.

Hausrat, T.J., Muhia, M., Gerrow, K., Thomas, P., Hirdes, W., Tsukita, S., Heisler, F.F., Herich, L., Dubroqua, S., Breiden, P., *et al.* (2015). Radixin regulates synaptic GABAA receptor density and is essential for reversal learning and short-term memory. *Nature communications* *6*, 6872.

Hirata, T., Suda, Y., Nakao, K., Narimatsu, M., Hirano, T., and Hibi, M. (2004). Zinc finger gene *fez*-like functions in the formation of subplate neurons and thalamocortical axons. *Developmental dynamics : an official publication of the American Association of Anatomists* *230*, 546-556.

Hla, T., Lee, M.J., Ancellin, N., Paik, J.H., and Kluk, M.J. (2001). Lysophospholipids - Receptor revelations. *Science* *294*, 1875-1878.

Hoerder-Suabedissen, A., and Molnar, Z. (2015). Development, evolution and pathology of neocortical subplate neurons. *Nature reviews Neuroscience* *16*, 133-146.

Hoerder-Suabedissen, A., Oeschger, F.M., Krishnan, M.L., Belgard, T.G., Wang, W.Z., Lee, S., Webber, C., Petretto, E., Edwards, A.D., and Molnar, Z. (2013). Expression profiling of mouse subplate reveals a dynamic gene network and disease association with autism and schizophrenia. *Proceedings of the National Academy of Sciences of the United States of America* *110*, 3555-3560.

Hoerder-Suabedissen, A., Paulsen, O., and Molnar, Z. (2008). Thalamocortical Maturation in Mice Is Influenced by Body Weight. *J Comp Neurol* *511*, 415-420.

Kanold, P.O., and Luhmann, H.J. (2010). The subplate and early cortical circuits. *Annual review of neuroscience* *33*, 23-48.

Kikuchi, S., Hata, M., Fukumoto, K., Yamane, Y., Matsui, T., Tamura, A., Yonemura, S., Yamagishi, H., Keppler, D., Tsukita, S., *et al.* (2002). Radixin deficiency causes conjugated

hyperbilirubinemia with loss of Mrp2 from bile canalicular membranes. *Nature genetics* *31*, 320-325.

Kingsbury, M.A., Rehen, S.K., Contos, J.J., Higgins, C.M., and Chun, J. (2003). Non-proliferative effects of lysophosphatidic acid enhance cortical growth and folding. *Nature neuroscience* *6*, 1292-1299.

Li, H., Fertuzinhos, S., Mohns, E., Hnasko, T.S., Verhage, M., Edwards, R., Sestan, N., and Crair, M.C. (2013). Laminar and columnar development of barrel cortex relies on thalamocortical neurotransmission. *Neuron* *79*, 970-986.

Liu, X., Huai, J., Endle, H., Schluter, L., Fan, W., Li, Y., Richers, S., Yurugi, H., Rajalingam, K., Ji, H., *et al.* (2016). PRG-1 Regulates Synaptic Plasticity via Intracellular PP2A/beta1-Integrin Signaling. *Developmental cell* *38*, 275-290.

Lopez-Bendito, G., Cautinat, A., Sanchez, J.A., Bielle, F., Flames, N., Garratt, A.N., Talmage, D.A., Role, L.W., Charnay, P., Marin, O., *et al.* (2006). Tangential neuronal migration controls axon guidance: a role for neuregulin-1 in thalamocortical axon navigation. *Cell* *125*, 127-142.

Lowery, L.A., and Van Vactor, D. (2009). The trip of the tip: understanding the growth cone machinery. *Nat Rev Mol Cell Bio* *10*, 332-343.

Matsui, T., Maeda, M., Doi, Y., Yonemura, S., Amano, M., Kaibuchi, K., Tsukita, S., and Tsukita, S. (1998). Rho-kinase phosphorylates COOH-terminal threonines of ezrin/radixin/moesin (ERM) proteins and regulates their head-to-tail association. *The Journal of cell biology* *140*, 647-657.

McConnell, S.K., Ghosh, A., and Shatz, C.J. (1994). Subplate pioneers and the formation of descending connections from cerebral cortex. *The Journal of neuroscience : the official journal of the Society for Neuroscience* *14*, 1892-1907.

Mills, G.B., and Moolenaar, W.H. (2003). The emerging role of lysophosphatidic acid in cancer. *Nature reviews Cancer* *3*, 582-591.

Ming, G.L., Song, H.J., Berninger, B., Holt, C.E., Tessier-Lavigne, M., and Poo, M.M. (1997). cAMP-dependent growth cone guidance by netrin-1. *Neuron* *19*, 1225-1235.

Mintz, C.D., Carcea, I., McNickle, D.G., Dickson, T.C., Ge, Y., Salton, S.R., and Benson, D.L. (2008). ERM proteins regulate growth cone responses to Sema3A. *The Journal of comparative neurology* *510*, 351-366.

Mire, E., Mezzera, C., Leyva-Diaz, E., Paternain, A.V., Squarzone, P., Bluy, L., Castillo-Paterna, M., Lopez, M.J., Peregrin, S., Tessier-Lavigne, M., *et al.* (2012). Spontaneous activity regulates Robo1 transcription to mediate a switch in thalamocortical axon growth. *Nature neuroscience* *15*, 1134-1143.

Mizuno, H., Luo, W., Tarusawa, E., Saito, Y.M., Sato, T., Yoshimura, Y., Itohara, S., and Iwasato, T. (2014). NMDAR-regulated dynamics of layer 4 neuronal dendrites during thalamocortical reorganization in neonates. *Neuron* 82, 365-379.

Molnar, Z., Adams, R., and Blakemore, C. (1998). Mechanisms underlying the early establishment of thalamocortical connections in the rat. *The Journal of neuroscience : the official journal of the Society for Neuroscience* 18, 5723-5745.

Morris, A.J., and Smyth, S.S. (2014). Lipid phosphate phosphatases: more than one way to put the brakes on LPA signaling? *Journal of lipid research* 55, 2195-2197.

Normand, E.A., Crandall, S.R., Thorn, C.A., Murphy, E.M., Voelcker, B., Browning, C., Machan, J.T., Moore, C.I., Connors, B.W., and Zervas, M. (2013). Temporal and mosaic Tsc1 deletion in the developing thalamus disrupts thalamocortical circuitry, neural function, and behavior. *Neuron* 78, 895-909.

Ohyama, K., Tan-Takeuchi, K., Kutsche, M., Schachner, M., Uyemura, K., and Kawamura, K. (2004). Neural cell adhesion molecule L1 is required for fasciculation and routing of thalamocortical fibres and corticothalamic fibres. *Neuroscience research* 48, 471-475.

Pearson, M.A., Reczek, D., Bretscher, A., and Karplus, P.A. (2000). Structure of the ERM protein moesin reveals the FERM domain fold masked by an extended actin binding tail domain. *Cell* 101, 259-270.

Petersen, C.C. (2014). Cortical control of whisker movement. *Annual review of neuroscience* 37, 183-203.

Pouchelon, G., Frangeul, L., Rijli, F.M., and Jabaudon, D. (2012). Patterning of pre-thalamic somatosensory pathways. *The European journal of neuroscience* 35, 1533-1539.

Ramesh, V. (2004). Merlin and the ERM proteins in Schwann cells, neurons and growth cones. *Nature reviews Neuroscience* 5, 462-470.

Riedl, J., Crevenna, A.H., Kessenbrock, K., Yu, J.H., Neukirchen, D., Bista, M., Bradke, F., Jenne, D., Holak, T.A., Werb, Z., *et al.* (2008). Lifeact: a versatile marker to visualize F-actin. *Nat Methods* 5, 605-607.

Schlatter, M.C., Buhusi, M., Wright, A.G., and Maness, P.F. (2008). CHL1 promotes Sema3A-induced growth cone collapse and neurite elaboration through a motif required for recruitment of ERM proteins to the plasma membrane. *J Neurochem* 104, 731-744.

Schwarz, Q., and Ruhrberg, C. (2010). Neuropilin, you gotta let me know: should I stay or should I go? *Cell Adh Migr* 4, 61-66.

Sheng, X., Yung, Y.C., Chen, A., and Chun, J. (2015). Lysophosphatidic acid signalling in development. *Development* 142, 1390-1395.

- Sigal, Y.J., McDermott, M.I., and Morris, A.J. (2005). Integral membrane lipid phosphatases/phosphotransferases: common structure and diverse functions. *Biochem J* 387, 281-293.
- Stukey, J., and Carman, G.M. (1997). Identification of a novel phosphatase sequence motif. *Protein Science* 6, 469-472.
- Tanaka, M., Kishi, Y., Takanezawa, Y., Kakehi, Y., Aoki, J., and Arai, H. (2004). Prostatic acid phosphatase degrades lysophosphatidic acid in seminal plasma. *FEBS letters* 571, 197-204.
- Tanaka, M., Okudaira, S., Kishi, Y., Ohkawa, R., Iseki, S., Ota, M., Noji, S., Yatomi, Y., Aoki, J., and Arai, H. (2006). Autotaxin stabilizes blood vessels and is required for embryonic vasculature by producing lysophosphatidic acid. *J Biol Chem* 281, 25822-25830.
- Tolner, E.A., Sheikh, A., Yukin, A.Y., Kaila, K., and Kanold, P.O. (2012). Subplate neurons promote spindle bursts and thalamocortical patterning in the neonatal rat somatosensory cortex. *The Journal of neuroscience : the official journal of the Society for Neuroscience* 32, 692-702.
- Tomsig, J.L., Snyder, A.H., Berdyshev, E.V., Skobeleva, A., Mataya, C., Natarajan, V., Brindley, D.N., and Lynch, K.R. (2009). Lipid phosphate phosphohydrolase type 1 (LPP1) degrades extracellular lysophosphatidic acid in vivo. *Biochem J* 419, 611-618.
- Trimbuch, T., Beed, P., Vogt, J., Schuchmann, S., Maier, N., Kintscher, M., Breustedt, J., Schuelke, M., Streu, N., Kieselmann, O., *et al.* (2009). Synaptic PRG-1 modulates excitatory transmission via lipid phosphate-mediated signaling. *Cell* 138, 1222-1235.
- Wright, A.G., Demyanenko, G.P., Powell, A., Schachner, M., Enriquez-Barreto, L., Tran, T.S., Polleux, F., and Maness, P.F. (2007). Close homolog of L1 and neuropilin 1 mediate guidance of thalamocortical axons at the ventral telencephalon. *The Journal of neuroscience : the official journal of the Society for Neuroscience* 27, 13667-13679.
- Xu, Y., Sari, Y., and Zhou, F.C. (2004). Selective serotonin reuptake inhibitor disrupts organization of thalamocortical somatosensory barrels during development. *Brain research Developmental brain research* 150, 151-161.
- Yamakado, M. (1995). Remodelling in the array of cell aggregates in somatotopic representation of the facial vibrissae through the trigeminal sensory system of the mouse. *Neuroscience research* 23, 399-413.
- Yamasaki, M., Okada, R., Takasaki, C., Toki, S., Fukaya, M., Natsume, R., Sakimura, K., Mishina, M., Shirakawa, T., and Watanabe, M. (2014). Opposing role of NMDA receptor GluN2B and GluN2D in somatosensory development and maturation. *The Journal of neuroscience : the official journal of the Society for Neuroscience* 34, 11534-11548.
- Yuan, X.B., Jin, M., Xu, X., Song, Y.Q., Wu, C.P., Poo, M.M., and Duan, S. (2003). Signalling and crosstalk of Rho GTPases in mediating axon guidance. *Nature cell biology* 5, 38-45.

Yung, Y.C., Stoddard, N.C., and Chun, J. (2014). Thematic Review Series: Lysophospholipids and their Receptors LPA receptor signaling: pharmacology, physiology, and pathophysiology. *Journal of lipid research* 55, 1192-1214.

Yung, Y.C., Stoddard, N.C., Mirendil, H., and Chun, J. (2015). Lysophosphatidic Acid signaling in the nervous system. *Neuron* 85, 669-682.

Zhang, X.F., Schaefer, A.W., Burnette, D.T., Schoonderwoert, V.T., and Forscher, P. (2003). Rho-dependent contractile responses in the neuronal growth cone are independent of classical peripheral retrograde actin flow. *Neuron* 40, 931-944.

# Curriculum vitae

## Jin Cheng

Tel: 0176-84322075 (mobile.de)    Email: jin.cheng@unimedizin-mainz.de

Institute of Microanatomy and Neurobiology,  
Johannes Gutenberg University Mainz  
Langenbeck strasse 1, 55129, Mainz, Germany

## CITIZENSHIP

Chinese

## EDUCATION

2013- present

**Doctor of Philosophy** (expected Jan. 2017)

Institute for Microscopic Anatomy and Neurobiology, University Medical Center,  
Johannes Gutenberg University, Mainz, Germany

Thesis: Precise Somatotopic Thalamocortical Axon Guidance Depends on LPA-Mediated  
PRG-2/Radixin Signaling

Supervisor: Dr. Johannes Vogt and Prof. Robert Nitsch

2006- 2009

**Master**

School of Chemical Engineering and Pharmacy, Wuhan Institute of Technology, Wuhan,  
China

Thesis: Homology modeling of insect and mammalian GABA receptors and insecticide  
design

Supervisor: Prof. Xiu-Lian Ju

2002- 2006

**Bachelor**

School of Chemical Engineering and Pharmacy, Wuhan Institute of Technology, Wuhan,  
China

Thesis: Synthesis study of the trihydroxy derivatives

Supervisor: Prof. Xiu-Lian Ju

## RESEARCH EXPERIENCE

2013 -present

### **Doctoral level**

Institute for Microscopic Anatomy and Neurobiology, University Medical Center,  
Johannes Gutenberg University, Mainz, Germany

Project: Molecular mechanism of PRG2 in thalamocortical projection

Supervisor: Dr. Johannes Vogt and Prof. Robert Nitsch

2012

### **Doctoral level**

Institute of Molecular and Cellular Anatomy, Ulm University, Germany

Project: Transcriptional regulation of neocortex development

Supervisor: Prof. Stefan Britsch

2009- 2011

### **Research Assistant**

Institute of Neurosciences, Chinese Academy of Sciences, Shanghai, China

Project: Structural basis for sustained activation of ASIC3 channels in responses to  
persistent acidosis

Constructed ASIC3 knock-in mouse line by gene targeting

Characterized transgenic mouse lines by behavior tests

Supervisor: Prof. Tian-le Xu

2006- 2009

### **Master's level**

School of Chemical Engineering and Pharmacy, Wuhan Institute of Technology, Wuhan,  
China

Project: Structure-based and Ligand-based drug design

Supervisor: Prof. Xiu-Lian Ju

## List of own publications

1. **Cheng J**, Sahani S, Hausrat TJ, Yang JW, Ji H, Schmarowski N, *et al.* Precise Somatotopic Thalamocortical Axon Guidance Depends on LPA-Mediated PRG-2/Radixin Signaling. *Neuron* **2016**, 92(1): 126-142.
2. Vogt J, Yang JW, Mobascher A, **Cheng J**, Li YB, Liu XF, *et al.* Molecular cause and functional impact of altered synaptic lipid signaling due to a prg-1 gene SNP. *EMBO molecular medicine* **2016**, 8(1): 25-38.
3. Wiegreffe C, Simon R, Peschkes K, Kling C, Strehle M, **Cheng J**, *et al.* Bcl11a (Ctip1) Controls Migration of Cortical Projection Neurons through Regulation of Sema3c. *Neuron* **2015**, 87(2): 311-325.
4. Wang X, Li WG, Yu Y, Xiao X, **Cheng J**, Zeng WZ, *et al.* Serotonin Facilitates Peripheral Pain Sensitivity in a Manner That Depends on the Nonproton Ligand Sensing Domain of ASIC3 Channel. *Journal of Neuroscience* **2013**, 33(10): 4265-4279.
5. Yang Y, Yu Y, **Cheng J**, Liu Y, Liu DS, Wang J, *et al.* Highly Conserved Salt Bridge Stabilizes Rigid Signal Patch at Extracellular Loop Critical for Surface Expression of Acid-sensing Ion Channels. *J Biol Chem* **2012**, 287(18): 14443-14455.
6. **Cheng J**, Ju XL. Homology modeling and atomic level binding study of GABA(A) receptor with novel enamione amides. *European journal of medicinal chemistry* **2010**, 45(9): 3595-3600.
7. **Cheng J**, Ju XL, Chen XY, Liu GY. Homology modeling of human alpha 1 beta 2 gamma 2 and house fly beta 3 GABA receptor channels and Surfex-docking of fipronil. *Journal of molecular modeling* **2009**, 15(9): 1145-1153.
8. Liu GY, Ju XL, **Cheng J**. Selectivity of Imidacloprid for fruit fly versus rat nicotinic acetylcholine receptors by molecular modeling. *Journal of molecular modeling* **2010**, 16(5): 993-1002.



9. Liu GY, Ju XL, **Cheng J**, Liu ZQ. 3D-QSAR studies of insecticidal anthranilic diamides as ryanodine receptor activators using CoMFA, CoMSIA and DISCOtech. *Chemosphere* **2010**, 78(3): 300-306.
  
10. Pan J, Liu GY, **Cheng J**, Chen XJ, Ju XL. CoMFA and molecular docking studies of benzoxazoles and benzothiazoles as CYP450 1A1 inhibitors. *European journal of medicinal chemistry* **2010**, 45(3): 967-972.

## Acknowledgements

I would like to express my deepest and sincere gratitude to [REDACTED] [REDACTED]. Since the first day I came to the lab, they provided me a stable and wonderful position. This makes me possible to invest all efforts to the research which I like very much. I appreciate their patient guidance, enthusiastic encouragement and useful critiques of this research work. Specially, I would like to thank [REDACTED], who discusses the project with me in the four years study and helps me correct my thesis.

I would also like to extend my thanks to [REDACTED], who cooperates with me to finish all western blot work in the thesis.

I am also grateful to [REDACTED], who discusses the project and gives me help in thalamus culture. Meanwhile, I am thankful to the technicians of the laboratory, [REDACTED] [REDACTED]. I take pleasure to thank all colleagues of the laboratory for all the kinds of help.

I am very grateful to all supervisors and professors for reviewing my Ph.D. defense.

Meanwhile, my special thanks go to [REDACTED], who always supports and encourages me in my difficult time.

Finally, I wish to thank my family for their support and encouragement throughout my study.

## Declarations

1. I hereby declare that the scientific work is being submitted for the award of the degree of Doctor of Philosophy (Ph.D.) at the Johannes Gutenberg-University Mainz. It has not been submitted to any other German or foreign university or comparable institution for the conferral of an academic degree.
2. I hereby declare that I have not unsuccessfully ended another doctoral or equivalent program in the subject area of the current doctoral program.
3. I hereby declare that I wrote the dissertation submitted without any unauthorized external assistance and used only sources acknowledged in the work. All textual passages which are appropriated verbatim or paraphrased from published and unpublished texts as well as all information obtained from oral sources are duly indicated and listed in accordance with bibliographical rules. In carrying out this research, I complied with the rules of standard scientific practice as formulated in the statutes of Johannes Gutenberg-University Mainz to insure standard scientific practice.

Jin Cheng  
5. 11. 2016